A REFRACTION STUDY OF THE MEDIAN RIDGE OF THE KANE FRACTURE ZONE

by

GEORGE MICAH CONNOR BLUMBERG

B.S., Mechanical Engineering
George Washington University
(1982)

Submitted to the Department of Earth, Atmospheric,
and Planetary Sciences in Partial Fulfillment of
the Requirements of
the Degree of Master of Science

at the

Massachusetts Institute of Technology

September 1987

Signature of Author_____
Department of Earth, Atmospheric, and Planetary
Sciences, June 1987

Certified by_____
Sean C. Solomon
Thesis Supervisor

Accepted by_____
William F. Brace
Chairman, Committee on Graduate Students

A REFRACTION STUDY OF THE MEDIAN RIDGE OF THE KANE FRACTURE ZONE

by

GEORGE MICAH CONNOR BLUMBERG

Submitted to the Department of Earth,
Atmospheric, and Planetary Sciences,
in partial fulfillment of the requirements
for the Degree of Master of Science

ABSTRACT

The median ridge of the Kane Fracture Zone is a 40 km long by 5 km wide feature that rises out of the eastern transform valley with 0.5 km of relief. Prompted by the desire to investigate the origin of this feature, a refraction experiment with an air gun source and a digital ocean bottom hydrophone receiver was conducted over the median ridge in 1985. The refraction data have been interpreted with travel time modelling and synthetic seismograms. The data are consistent with a highly thinned crust, about 3 km thick, and an absence of a well-developed layer 3. The record section and best-fitting velocity model resemble those from the aseismic fracture zone trough to the east of the ridge-transform intersection, a segment of fracture zone devoid of a median ridge. The median ridge is thus underlain by substantially thinner crust than that beneath the transform trough to the immediate south, which is 6-7 km thick on the basis of earlier refraction data. A number of models for the formation of median ridges are considered, including uplift by serpentinization of the upper mantle, uplift by horizontal compressive stresses operating across the transform, intratransform volcanic construction, and thermal uplift. None of these models provide a straightforward explanation for the seismic structure of the median ridge and adjacent transform trough. Several future experiments that might sharpen and discriminate among competing models are suggested.

Thesis supervisor: Sean C. Solomon, Professor of Geophysics

Acknowledgements

The generous involvement of several people made this project possible. I would first like to thank my parents and siblings for their consistent support and concern. My advisor, S. C. Solomon deserves my most sincere thanks for his tireless effort in correcting my dismal prose, encouragment, generosity, and bounteous support. G. M. Purdy deserves a lion's share of credit for this thesis. He provided the data, computer services, technical support, many fine conversations and the opportunity to find adventure at sea and in foreign ports. To Dave Dubois, who maintains the W.H.O.I. seismic data reduction laboratory to such high standards, I would like to offer my warm thanks for his patience and perseverance in the face of an endless stream of questions. I would like to thank those who have helped by contributing through thoughtful suggestions: Joe Cann, Henry Dick, Brian Tucholke and Hans Schouten, and to Doug Toomey who gave me space in his office at Woods Hole. Special thanks for Peter Argyres, Jim Broda, Walter Cook, Carlton "Butch" Grant, Don Koelsch, F.Beecher Wooding, for camaraderie at sea and for help in collecting the data. I would like to thank Greg Beroza, Mark Murray, Bob Grimm and Justin Revenaugh whose contributions often came in very strange forms. Thanks especially to Laura Doughty for magnanimously helping in the multiple revisions of the manuscript and to Janet Sahlstrom who provided a most important job: strong administrative support. The other contributors who gave their time and energy to keep me thinking straight are Lippman Geronimus, Susan Leeman, David Silverman, Jim Mendelson and to the residents of 18 Nonantum Place in the city of Newton. I dedicate this thesis to James Marshall, who became involved at the very beginning of my life and never lost interest. This research was supported by the National Science Foundation under grants EAR-8416192 and EAR-8617967.

TABLE OF CONTENTS

INTRODUCTION

Fracture zones offset the axis of mid-ocean ridges (Figures 1 and 2) and display some of the most rugged relief of the ocean floor. Their kinematic role as transform faults [*Wilson*, 1965] was confirmed by fault plane solutions of earthquakes [*Sykes*, 1967], which show that strike-slip motion along the fault is opposite to the sense of the offset of the ridge axis (Figure 3). Fracture zones also play an important role in the thickness and composition of oceanic crust [*Karson and Dick*, 1983; *Fox and Gallo*, 1984]. Because of the spacing between fracture zones and the width of their zone of influence, as much as 20% of all crust generated along slow-spreading ridges is affected by fracture zone processes [*H. J. B. Dick*, personal communication, 1986].

Although fracture zones display a great many morphotectonic forms, it is generally accepted that each is composed of two principal tectonic elements [*Fox and Gallo*, 1984]: the seismically active zone of strike-slip tectonism joining the two offset ridge axes, and the two aseismic or fossil limbs (Figure 3). Characterized by linear depressions 4-6 km deep and tens of kilometers across, the fossil limbs of the fracture zone appear as continuous features for distances up to several thousand kilometers from the ridge axis and may persist across the full width of an ocean basin.

Recent studies of fracture zone physiography have led to a generalized classification of morphological domains [*Fox and Gallo*, 1984]. The fracture zone domain is defined as the broad band of transform-parallel topography, the portion of the ridge parallel topography that deepens as it approaches the transform, and

the two aseismic limbs of the fracture zone. This domain contrasts markedly with the fault-controlled, ridge-parallel structures generated at the accreting axis. As an intersection with a major transform is approached along the Mid-Atlantic Ridge, the seafloor deepens from 2-3 km along the ridge to as much as 5-6 km in the nodal deeps at the intersection. This bathymetric transition occurs over a distance of tens of kilometers. The transform portion of the fracture zone domain is dominated by a deep valley of inward facing slopes; the transform valley is generally shallower than the nodal deeps [*Fox and Gallo,* 1984].

Within the transform valley the wide swath of disturbed topography related to transform faulting, referred to as the Transform Tectonized Zone (TTZ), has been identified at fracture zones using GLORIA side scan sonar [*Lonsdale*, 1978; *Searle*, 1983] and observations from submersibles [*Karson and Dick,* 1983; OTTER, 1984, 1985]. The TTZ (Figure 4) is taken to represent the maximum width of the seafloor affected by transform fault tectonism. Features common to the TTZ include strike slip faults as well as ancillary dip-slip scarps [*Francheteau et al.,* 1976; *Lonsdale*, 1978; *Searle*, 1979; *CYAMEX Scientific Team and Pastouret,* 1983; *Karson and Dick*, 1983].

Within the deformed terrain an area of observable fault and scarp traces exists that is known as the transform fault zone (TFZ). This zone is thought to include the area most recently affected by strike slip tectonism [*Fox and Gallo,* 1984]. If a single fault or scarp can be traced along the TFZ this can be assumed to be the principal locus of present fault motion. This single fault trace is known as the Principal Transform Displacement Zone (PTDZ) [*Fox and Gallo*, 1984].

Refraction studies reveal that the crust in fracture zones is markedly different from "normal" oceanic crust. Generally, the seismic velocity is lower, a distinct seismic layer 3 is absent, and the crust is considerably thinner than elsewhere [*Detrick and Purdy,* 1980; *Ludwig and Rabinowitz,* 1980; *Detrick et al.*, 1982; *Sinha and Louden,* 1983; *Cormier et al.,* 1984; *Whitmarsh and Calvert*, 1985; *Calvert and Potts,* 1985; *Potts et al.*, 1986; *Louden et al.*, 1986].

Within the transform valley a dynamically maintained zone of faulting and fissuring has led to the juxtaposition of rocks of different histories and ages as well as the appearance of uplifted slivers of crust. A wide range of rocks have been dredged from within the fracture zone domain. Rocks recovered include diverse suites of gabbros and ultramafics, rocks that are commonly associated with the lower portions of the oceanic crust and uppermost mantle [*Karson and Dick,* 1983]. The circulation of water deep into the crust and the accompanying hydrothermal alteration of crustal and upper mantle rocks [*Francis*, 1981] may also be important at fracture zones.

A variety of models have been proposed to account for the huge relief observed at fracture zones, the anomalous rocks recovered along fracture zone scarps, and the gradual deepening of the ridge axis as the fracture zone is approached. One proposal is that the magma supply along a ridge occurs in cells initiated by a Rayleigh-Taylor instability in a layer of rising magma [*Whitehead et al.*, 1984; *Schouten et al.*, 1985]. By this hypothesis, magma supply varies along the accreting axis and is diminished near the fracture zones [*Schouten and Klitgord,* 1982; *White*, 1983; *White et al.,* 1984; *Whitehead et al.*,

1984] where the accretion axis is juxtaposed against cold, older lithosphere [*Fox and Gallo,* 1984]. Fracture zones have also been modeled as thermal cracks in the ocean floor [*Collette*, 1974; *Turcotte*, 1974] and as a large number of small-throw faults with relief from a few centimeters to tens of meters making up the fracture zone terrain [*Francheteau et al.,* 1976].

Prominent along many fracture zones are elongate, elevated ridges that strike parallel to the fracture zone trough (Figures 3 , 4 and 6). These ridges occur both as median ridges within the active transform valley floor and as transverse ridges located adjacent to the fracture zone trough. Because of their comparatively modest relief (500 m), width (1-5 km), and linear extent (40 km), median ridges have only recently been recognized. It was not until the advent of the multi-narrow beam sonar imaging (Sea Beam) (Figure 5) and Global Positioning Satellite (GPS) navigation system that practical experiments could be conducted over such small features. Many transforms slipping at a wide range of rates are now known to contain some form of median ridge structure; including the Blanco, Orozco, Clipperton [*Gallo et al.,* 1986], Garrett, Charlie-Gibbs, Kane, and Vema [*Macdonald et al.,* 1986] transforms. The median ridge of the Kane Fracture Zone (Figures 5 and 6) is the topic of this thesis.

Like the larger transverse ridges that are often found on the flanks of large Atlantic transforms, median ridges are believed to have undergone rapid vertical movement [*Bonatti*, 1978; *Gallo et al.,* 1986]. Reflection seismic records indicate an upturning of sedimentary layers against the median ridge in the central Vema transform; this result constitutes evidence for recent vertical movement at rates of

0.4-0.7 mm/yr [*Kastens et al.,* 1986; *Macdonald et al.*, 1986].

Recognizing that median ridges may be a feature common to fast and slow slipping transforms and that the origins of these features may be related to the processes of creation and modification of oceanic crust near fracture zones, a refraction study was carried out in July 1985 during cruise 180 of the R/V Knorr to determine the seismic velocity structure of the median ridge within the transform portion of the Kane Fracture Zone. In this thesis we present an analysis of the data from that experiment and an interpretation of the results in terms of current models for the nature and origin of fracture zone median ridges.

THE KANE FRACTURE ZONE

The Kane Fracture Zone in the north Atlantic Ocean offsets the Mid-Atlantic Ridge by 160 kilometers in a left lateral sense (Figure 2). The active transform portion of the fracture zone is located between 23 and 24°N and 45 and 46°W (Figure 1). In terms of its morphological, geological and geophysical characteristics, the Kane appears to be typical of long-offset (>100 km), slow-slipping (2-4 cm/yr) transform faults [*Karson and Dick,* 1983]. Magnetic data confirm that the Kane Fracture Zone has been a distinct feature since at least 80 My ago and probably since the early opening of the Atlantic [*Schouten and Klitgord*, 1982].

The Kane transform is clearly defined as a deep valley, with an overall strike of N100°E (Figure 5). The easternmost 45 km of the valley floor contains a distinct median ridge having the same trend as that of the transform as a whole (Figure 5). The walls of the transform valley are characterized by the plunging ridges and valleys of the ridge-parallel fabric. Differences exist between the northern and southern valley walls. To the north of the median ridge, the ridge-parallel troughs and ridges plunge onto the valley floor and terminate as closed contour depressions that are possibly relict nodal basins originating from the western ridge transform intersection [*Pockalny et al.,* 1987]. At the southern wall of the transform adjacent to the median ridge, in contrast, the ridge-parallel topography terminates as large block-like features rather than the gradual plunging as seen to the north (Figure 6). The southern wall is much steeper and shallower than the northern wall . A narrow undulating plain 1-2 km wide with an

average depth of 4200 m separates the base of the median ridge from the base of the southern fracture zone wall. A closed contour depression (possibly a relict nodal deep) is at the west end of the plain and adjacent to the median ridge. The ridges and troughs that descend the northern and southern walls of the transform valley do not appear to transect the median ridge. This may be an indication that the median ridge is a part of the separate fabric of the transform valley and is tectonically distinct from the bordering ridge-generated lithosphere.

The central portion of the median valley, to the west of the median ridge, lacks a strong morphotectonic fabric [*Pockalny et al.,* 1987]. Slender, low (less than 100 m relief) transform-parallel ridges line the floor of the valley. These lineaments are well represented in the GLORIA sonographs [*Searle*, 1986]. The western 25 km of the valley floor is the site of a much smaller median ridge, with only about 200-300 m of relief.

The north-south trending ridges and troughs that make up the fracture zone valley walls serve as regional strain markers [*Pockalny et al.*, 1987]. The ridges and troughs exhibit little lateral deformation or evidence of strike-slip motion at distances as small as 3 km from the transform valley axis. This indicates that the major locus of strike slip motion, the TTZ, is confined to a band no more than 6 km wide at the ends of the transform and as narrow as 2 km wide in the center. A zone, 2-4 km wide, of generally parallel lineaments observable on GLORIA sonar images (Figure 7) supports this interpretation [*Searle*, 1986].

Unfortunately, the Sea Beam map of the Kane [*Pockalny et al.*, 1987] and the GLORIA interpretation [*Searle*, 1986] give no definitive indication of the location

of the PTDZ. *Garfunkel* [1986] and *Pockalny et al.* [1987] suggest that the PTDZ follows a straight line connecting the ends of the neovolcanic zones at each ridge-transform intersection. The median ridge in the eastern transform is to the north of the suggested PTDZ, while the median ridge in the western transform is to the south of this line. The inferred PTDZ passes across a section of the transform valley that has no pronounced median ridge but has strong transform-parallel lineaments as inferred by the GLORIA sonographs (Figure 7). Although the direction of transform motion implied by this choice of PTDZ (N98°E) is within the 2-σ error in the value (N100°E) predicted from plate motion model RM2 [*Minster and Jordan*, 1978], *Garfunkel* [1986] has suggested that the 2-4° difference may be significant and may imply that the Kane transform is in a leaky mode.

Narrow TFZ's and prominent PTDZ's appear more common in fast-slipping transforms in the Pacific. In large-offset, slow-slipping transforms like the Kane (Figure 5), broader and more complicated patterns appear to make up the TFZ [*Searle*, 1986]. The TFZ's may be narrower and more concentrated at the base of median ridges such as in the Vema transform [*Macdonald et al.*, 1986]. It is unclear what tectonic role, if any, is played by the median ridge in the TFZ. The median ridges may guide the locus of most recent faulting, or they may simply mask the complicated fault patterns as a result of uplift, mass wasting or tectonic rearrangement [*Macdonald et al.*, 1986].

The Kane appears to be at one extreme of the range of fault zone widths among large-offset Atlantic transforms. It has been suggested that there is a

correlation between the width of the transform tectonized zone and the angle the adjacent ridge axis makes with the plate spreading direction [*Searle*, 1986]. Generally the more oblique the angle, the thinner the TFZ. According to *Searle* [1986] the width of the TFZ ranges from 1.5-2 km for the Charlie-Gibbs, at which the Mid-Atlantic Ridge makes an angle of 42° to the spreading direction, to 2-4 km for the Kane, which meets the ridge at an angle of about 90°.

Considerable emphasis has been placed by other researchers on the possibility of changes in the direction of relative motion across transform faults because a significant amount of tectonic rearrangement would result. Major changes in the direction of slip along the Kane transform have been documented from bathymetric trends and magnetic anomalies [*Fox et al.*, 1969; *Rabinowitz and Purdy*, 1976; *Purdy et al.*, 1979; *Collette et al.*, 1984; *Tucholke and Schouten,* 1985; *B. E. Tucholke*, unpublished map, 1987]. It has been suggested that the Kane was subjected to major directional changes at 5, 2.5, and 0.5 My ago [*Tucholke and Schouten,* 1987].

The Kane Fracture Zone has also undergone major structural changes in the more distant past. Variations in the depth to basement along the aseismic limbs of the fracture zone indicate fault trace offsets and blockages by basement highs on both limbs of the fracture zone [*Tucholke and Schouten,* 1987]. Asymmetric spreading has occurred on the ridge segments to the north (half rates of 14 and 13 mm/yr to the west and east, respectively) and south (16 and 12 mm/yr to the west and east, respectively) of the Kane; as a result of this asymmetry the transform offset has been increasing by 10 km/My in the past 20 My [*Purdy et al.*,

1979; *Schouten et al.*, 1979]. As noted above, a state of tension may have existed across the Kane for the past 20 My [*Tucholke and Schouten*, 1987].

A median ridge of the scale observed in the transform valley today is not observed on maps of depth to basement within the fossil trace of the fracture zone [*Tucholke and Schouten*, 1987]. Conventional wide-beam echo sounder records show no median ridge for at least 200 km to the east of the intersection [*G. M. Purdy,* personal communication, 1987]. More shallow reflection studies are needed to determine if fine-scale median ridges exist outside the transform, perhaps buried under debris or sediment. This result would have important implications for the evolution and origin of the ridge feature.

The median ridge in the eastern Kane transform was dredged twice on Cruise 180 R/V Oceanus in January 1987. Recovered rocks included unmetamorphosed pillow basalt, greenschist-facies metabasalt (brecciated pillow basalt hydrothermally altered) and brownstone-facies aphyric metabasalt [*C. Langmuir*, personal communication, 1987]. The relationship of these hydrothermally altered basalts and breccias to the large-scale structure of the median ridge is not clear. Observations with D.S.R.V. Alvin [*Karson and Dick,* 1983] at the ridge-transform intersection have shown that the neovolcanic zone crosses the nodal basins and terminates against the opposite wall of the fracture zone. The dredged rocks may also have simply fallen from the walls above the valley before the median ridge was uplifted.

Although no upper mantle peridotites or serpentinites were found in dredge hauls from the median ridge, samples of upper mantle rocks have been

recovered nearby. The inactive portion of the Kane Fracture Zone to the east of the eastern ridge-transform intersection was dredged successfully on Cruise 96 of the R/V Atlantis II in 1977. The rocks recovered contained a significant proportion of peridotites and basalts. Close inspection from Alvin [*G. Thompson*, personal communication, 1986] showed the presence of serpentinized peridotite intrusions on the walls of the aseismic limb of the fracture zone south of the eastern ridge-transform intersection.

Several seismic experiments have been carried out to date along the Kane Fracture Zone and its intersection with the Mid-Atlantic Ridge [*Detrick and Purdy,* 1980; *Cormier et al.,* 1984; *Purdy and Detrick,* 1986]. Significant variations in crustal structure appear to be present along the fracture zone. The fracture zone valley to the east of the ridge-transform intersection is underlain by crust only 2-3 km thick to a distance of 300 km from the intersection. The thickest crust (5-6.5 km) is found adjacent to (to the immediate east and west of) the ridge-transform intersection and in the deepest portion of the valley south of the median ridge. Although thinned, this crust is more similar to "normal" crust found away from fracture zones. Delay-time experiments suggest that the pronounced thinning of the crust occurs very abruptly as the fracture zone is approached and is confined to a zone about 10 km in width [*Detrick and Purdy,* 1980; *Cormier et al.*, 1984]. More gradual crustal thinning may extend to distances of tens of kilometers from the fracture zone [*Cormier et al.,* 1984; *Purdy and Detrick,* 1986]. The nodal deep appears to be the location of the thinnest crust, perhaps as thin as 1 km [*Cormier et al.,* 1986]. Refraction results in the median valley to the south of the Kane

transform show normal (6-7 km) thickness crust beneath much of the inner floor with thinner crust confined to a transitional zone 30 km from the transform intersection [*Purdy and Detrick,* 1986].

A detailed gravity study was conducted at the Kane and interpreted using a spectral analysis approach [*Louden and Forsyth,* 1982]. The gravity and topography are best explained by a model in which loads are supported by the flexural rigidity of the lithospheric plate. Unfortunately, shorter wavelength features, like the median ridge, have been difficult to model. More fine-scale, two dimensional gravity studies are needed in order to observe and model such small features.

HYPOTHESES FOR THE FORMATION OF MEDIAN RIDGES

A number of hypotheses have been advanced to account for the creation of transverse and median ridges within the fracture zone domain. These include: diapirism of altered upper mantle material, the effects of compressional and tensional stresses in the fracture zone domain, and thermal conduction across fracture zones. Each hypothesis is described below and will be evaluated with respect to the median ridge at the Kane Fracture Zone. We specifically seek predictions of each hypothesis testable by seismic refraction. Of course, these processes need not be mutually exclusive, and we should be open to the possibility that several mechanisms work sequentially or simultaneously to produce median ridges.

Diapirism

Serpentinized peridotites are among the most commonly dredged rocks from the ocean floor. They have been found at a variety of settings [*Rona et al.,* 1987], including: (1) ridge-parallel scarps at distances greater than 30 km from the ridge axis in the Atlantic [*Bonatti and Hamlyn,* 1981] and the Red Sea [*Bonatti et al.,* 1986], (2) median valley walls along the Mid-Atlantic Ridge [*Bonatti et al.*, 1975; *Karson et al.*, 1986], (3) walls of the aseismic limbs of fracture zones on the Mid-Atlantic Ridge [*Bonatti and Hamlyn,* 1981], (4) walls bordering transform faults at large-offset (>100 km) transforms on the Mid-Atlantic [*Bonatti and Hamlyn*, 1981; *Michael and Bonatti*, 1985] and Southwest Indian Ridge [*Engel and Fisher,* 1975] and the East Pacific Rise [*Hebert et al,* 1983], (5)

ridge-transform (RT) and ridge-nontransform (RN) corners (Figure 3) in the Atlantic [*Karson and Dick*, 1983; OTTER, 1984; *Rona et al.*, 1987], and (6) walls of ocean trenches and back-arc basins [*Bonatti and Hamlyn*, 1981]. It is noteworthy for this study that serpentinized peridotites have been recovered from both transverse ridges [*Thompson and Melson*, 1972; *Bonatti*, 1976; *Bonatti and Honnorez*, 1976] and at least one median ridge [*H. J. B. Dick*, unpublished data from the Atlantis II Fracture Zone] in large-offset slow-slipping fracture zones.

Serpentinites form through hydration of upper mantle peridotite. Reactions of olivine and pyroxene with water lead to the formation of serpentine at temperatures below 500°C [*Bonatti*, 1976]. Isotopic studies of serpentine have suggested that large quantities of seawater drive the reaction. Depending on the degree of serpentinization a density decrease by as much as 25% can accompany the reaction [*Coleman*, 1970]. Such a density change can initiate a gravitational instability, or diapir, leading to the formation of a ridge (Figure 8) [*Kingma*, 1958; *Bonatti*, 1978] .

Diapirs appear to originate preferentially near zones of weakness in the oceanic crust, notably along fracture zones. Water penetration within the transform valley is feasible considering the extent of fissuring and faulting [*Francis*, 1981; *Gregory and Taylor*, 1981]. The observation of serpentinite at the RT corner (Figure 3) of fracture zones may indicate that diapirism occurs within 1 My of the formation of oceanic crust. This diapirism can have dramatic results. St. Peter's and St. Paul's Rocks, for instance, at St. Paul's Fracture Zone in the equatorial Atlantic (Figure 1) appear to be solid plugs of serpentinized peridotite

surrounded by oceanic crust [*Melson et al.*, 1967].

The amount of serpentinite recovered at fracture zones appears to be inversely proportional to the spreading rate [*Dick*, 1986], suggesting that the formation or transport of serpentinite is related to the tectonics of the ridge-transform intersection. Along the very slow-spreading Southwest Indian Ridge where magma supply is low and the crust is thought to be relatively thin, serpentinites comprise 64% of the recovered samples [*Dick*, 1986]. Along the fracture zones of the Mid-Atlantic Ridge dredging yields, on average, 10-30% serpentinite. On fracture zones of the fast-spreading East Pacific Rise, in contrast, only a few percent of the samples recovered are serpentinized peridotites.

The density and seismic velocities of serpentinized peridotites have been determined by laboratory experiment as functions of the degree of serpentinization and pressure [*Christensen*, 1966, 1972; *Fox et al.*, 1973, 1976]. Representative results are shown in Figure 9. Not suprisingly, the degree of serpentinization has a large effect on seismic velocities. P-wave velocity ranges from approximately 8 km/s for pure peridotite to less than 5 km/s for 100% serpentine at a pressure of 2 kbar (Figure 9). Seismic methods, therefore, are often confounded by serpentinized rocks since the degree of serpentinization is variable and the P-wave velocity may be similar to that of basalt or gabbro. Shear wave analysis can, in principle, help to remove this ambiguity, since a large Poisson's ratio can be diagnostic of a significant degree of serpentinization [*Christensen*, 1972].

A variety of models involving partial to complete serpentinization of portions of the upper mantle are possible, with trade-offs among percent serpentinization, the thickness of the involved mantle layer, and the resulting seafloor relief. Several such simple models are considered in Figure 10. Model (a) consists of a column of crust uplifted by a layer of serpentinized peridotite. Isostatic considerations mandate that for a layer of 100% serpentinized peridotite and for assumed densities of 2.55 g/cm^3 for serpentine [*Coleman*, 1970] and 2.9 and 3.3 g/cm^3 for unmodified crustal and mantle material, respectively, a 500-m elevation for the median ridge requires a serpentinized layer 1.5 km thick. P-wave velocity for the serpentinite layer would be about 5 km/s; if this layer underlays a 3-km section of thinned fracture zone crust [*Cormier et al.,* 1984] the depth to normal mantle would be 4.5 km. Of course, the depth to unmodified mantle would be greater if the crustal layer were thicker or if the degree of serpentinization were less than 100 %.

In model (b) the median ridge is underlain only by a serpentine diapir, without an overlying crustal layer. For a thickness of 3 km for the surrounding crust [*Cormier et al.*, 1984], a column of 100% serpentinized peridotite would be 3.1 thick to yield 500 m of relief and would have a P wave velocity of about 5 km/s. Somewhat greater thicknesses and velocities are permitted by lesser degrees of alteration.

Model (c) represents the case where more normal thickness (6.5 km) crust flanks the median ridge. The median ridge is assumed to consist of thinned fracture zone crust [*Cormier et al.*, 1984] with a layer of serpentinized peridotite

beneath. Uplift of 0.5 km could be achieved in this case with a 3.4-km-thick layer of serpentine under the thinned crust. The velocity structure of this model would indicate a crustal section about 6-7 km thick with lower crustal velocities of about 5 km/s. Again, the total thickness and lower crustal velocity would both be greater for a lower degree of serpentinization.

Model (d) explores the possibility that the median ridge is underlain by a completely serpentinized section of upper mantle surrounded by partially serpentinized upper mantle of the same thickness (3 km). The median ridge would have 0.5 km of relief if the surrounding material were 45% serpentinized. The P wave velocity in the crust beneath the median ridge would be about 5 km/s, while that beneath the surrounding regions would be about 6 km/s (Figure 9).

The models of Figure 10 are merely examples of a wide variety of structures compatible with the serpentinization hypothesis as well as with local isostatic equilibrium. Seismic velocity structure beneath the median ridge and adjacent crustal regions and gravity profiles across the transform would all contribute to distinguishing among the models.

Transfer of horizontal stress

Regions of extensional and compressional stress, resulting from a number processes, may contribute to vertical tectonism in a fault zone [*Bonatti*, 1978; *Segal and Pollard*, 1980]. If compressive stresses are sufficiently high then thrust faulting or lithospheric flexure can lead to uplift or folding within the fracture zone

valley. Extension across the transform may open fissures and faults which allow magma to intrude the transform zone, leading to a volcanic edifice. As noted above, such fracturing may also allow water to percolate to mantle depths, leading to serpentinization and to diapirism.

Several factors can contribute to changes in the normal stress across a fracture zone. These include changes in the direction of spreading [*Menard and Atwater,* 1968, 1969], differential thermal contraction [*Collette*, 1974; *Sandwell and Schubert*, 1982; *Sandwell*, 1984], and flexure [*Parmentier and Haxby*, 1986]. An anastomozing network of faults along the TFZ may also lead to local regions of extension (pull-apart basins) and compression (uplifted blocks) similar to those observed along strike-slip fault zones on the continents [*Segal and Pollard*, 1980; *Mann et al.,* 1983]. The effect of this type of uplift on the velocity structure of the median ridge may be very subtle since the shearing and thrusting involved is fundamentally mechanical in nature, and the resulting velocity structure might differ only slightly from that of surrounding regions. Thrusting induced by horizontal compressive stress might be discerned in a refraction study only if significant crustal thickening resulted.

Intratransform volcanic construction or formation of new crust within a leaky transform (Figure 11) might be difficult to distinguish seismically from crust formed at the ridge-transform intersection. Dredge hauls dominated by fresh, glass-rimmed basalt would support a volcanic constructional origin for a median ridge.

Lateral heat transport

Fracture zones have a complex thermal regime due to the juxtaposition of the hot accreting axis against a colder, thicker section of lithosphere. *Bonatti* [1978] proposed that vertical uplift of a transverse ridge would result from the transfer of heat across the fracture zone. *Phipps Morgan and Forsyth* [1987] modeled the thermal structure of a ridge-transform intersection and concluded that the thermally-induced uplift for a transform with a 10 My offset would be 200-300 m. This model predicts that the maximum uplift would occur 30-40 km from the intersection on the aseismic fracture zone limb. Presumably, seismic velocities would be slightly reduced by reheating, but the crustal thickness would be unmodified. This model does not account for the uplift of a feature as small as the median ridge, located within the center of the transform valley.

EXPERIMENT DESCRIPTION

A refraction experiment was conducted from the R/V Knorr in 1985 over a 14 km length of the Kane Fracture Zone median ridge using a digital ocean bottom hydrophone [DOBH, *Koelsch et al.*, 1982] and a 1000 in^3 air gun. Over 400 shots were recorded during four passages along the shooting line (Figures 5 and 7). Navigation was with GPS. The dense spacing of the shots (0.1 km) permitted stacking of seismograms with similar ranges to boost the signal-to-noise ratio and improve resolution. The length of the air gun line (14 km), the spatial density of shots along that line (approximately every 0.1 km), and the wavelength of P waves in the crust (approximately 300 to 600 m) define the scale of the resolvable seismic structure.

The source waveform of the air gun is one of several factors that determine the spatial resolution of the experiment. Because of seafloor reflections, the water wave recorded directly by the DOBH is not a good image of the source. Fortunately, another experiment conducted on the same cruise yielded a measurement of the uncontaminated direct water wave signal (Figure 12). It can be seen in this figure that the predominant frequency of the 1000 in^3 air-gun is about 9 Hz when towed astern of the ship at a depth of 10 m with air supply regulated at 1750 ± 100 lbs/in^2. An electronically activated release valve allows accurate timing of the shot; shot instant errors are negligible. Due to the short duration of this experiment and the high accuracy of the instrument clock (0.09 ms drift), errors due to timing offset between shooting and receiving stations are also negligible.

The DOBH was preprogrammed to be in several different modes of data collection during the course of this single experiment. Two digitizing rates were used: 200 and 2000 samples per second. The latter data rate was judged too high for this experiment; these data were decimated prior to further analysis. The decimation was accomplished by fitting a cubic spline to the data and resampling at 200 samples per second, making all the data compatible, an essential step for stacking. An anti-alliasing Butterworth filter was applied before decimating; the cut off frequency was at 100 Hz and the rolloff was 64 db/decade.

The location of the DOBH on the seafloor was estimated from the location of the ship at deployment. The experiment was conducted entirely within the 12 hour period during which GPS was operational so that ship and source positions were accurate to within a few tens of meters.

Ranges from the shots to the DOBH were determined independent of the ship and receiver positions from the water wave travel times, under the assumption that the water wave path is a straight line. A nearby CTD cast was used to determine the water column velocity of 1.509 km/s. Water wave arrival time errors and variations in the sounding velocity contribute to errors in the range determination, but these are generally small (10-20 m).

Because of the relatively weak signal of the air gun source, the technique of stacking waveforms was used to improve the signal to noise ratio. Because the ship followed the same track accurately on repeated passes over the ridge, ray paths were assumed to lie in a common plane. To confirm this, travel time picks, record sections and topographic profiles (Figure 13) were overlaid and

compared. It was determined that the four different ship tracks were sufficiently close that differences in the record sections caused by differences in topography are slight.

In the stacking procedure, traces were binned by range into segments of 120 m width. All seismograms in a bin were summed, after delaying or advancing the time scale depending on whether the seismogram range was greater or less than the center of the bin. The delay or advance correction was based on a velocity characteristic of the refracted arrivals. Since four air gun tracks were run over the median ridge, the signal to noise ratio was enhanced by about a factor of two by this procedure. The stacked record section is shown in Figure 14.

Travel time picking errors are commonly a large source of uncertainty in seismic interpretation. A technique was adopted for picking the same phase consistently from all sections. A prominent trough or peak of interest was followed across the section. A standard correction was applied to make all arrival time picks for this phase consistent . The long, ringing bubble-pulse signal of the air-gun source (Figure 12) makes this technique possible. This technique allows the possibility of a systematic bias of ~0.05 s in all travel times. Such a bias will map only into the shallowest structure, however, and will not affect the estimation of the phase velocity of prominent arrival branches.

In order to make accurate topographic corrections an assumption about the variations of subsurface velocity structure with seafloor depth must be made. Two different assumptions on the layering of sub-seafloor structure are commonly made. *Kennett and Orcutt* [1976] used a method, known as the water path

correction, which removes the travel times within the water layer assuming that sub-bottom layering is conformal to the seafloor. *Whitmarsh* [1979] advocated a water delay correction technique, in which the water layer is retained but the seafloor is effectively flattened to a common datum. The water path correction is considered the most appropriate since it makes no assumptions about the basement structure and effectively places the shots on the seafloor [*Purdy*, 1982]. The water path correction was therefore employed for this data set.

Errors in the water path correction contribute a large uncertainty to the data reduction procedure. Accurate values of water depth must be obtained from the echo sounder record. Since the ship traversed the median ridge, side echos were not observed and the depth under the ship can probably be determined to a precision of less than 10 m. A cubic spline was fit to the bathymetric profiles, and this curve was used with the appropriate phase velocity to estimate the depth and position of ray entry points.

Water path corrections were applied independently to travel times from each of the four air gun lines. The corrected travel times were merged into a single data set (e.g., Figure 15b). The variance in the travel time data at each range should be a measure of random errors in the travel time readings and their topographic corrections, as well as errors introduced by unmodeled lateral heterogeneity in the velocity structure. At 2-4 km range the travel times have a sample standard deviation of $\pm$ 0.02 s; at 6-10 km range the travel time standard deviation is $\pm$ 0.01 s. These uncertainties provide a basis for evaluating the fit to the observations of travel times predicted by velocity models.

ANALYSIS OF RESULTS

In the final stacked record section (Figure 14) two prominent refracted arrival branches are evident. The first branch (2-6 km range) has a velocity of about 4.0 km/sec; the second branch (7-12 km range) has a velocity of about 6.5 km/sec. A complex phase reversal due to triplication appears to occur at a range of about 7 km; this feature was an important constraint on our modeling .

The amplitude characteristics of the data set are very distinctive. Amplitudes are high at short ranges (near 2 km) when the first refracted branch breaks out of the water wave. Arrivals at ranges of 6.5-7.5 km exibit very low amplitudes, while larger amplitude appear at ranges greater than 7.5 km. Moderate amplitudes persist to a range of 12 km where they gradually diminish. No arrivals with upper mantle velocities were recorded; this may indicate that the velocity gradient in the uppermost mantle is too small to refract waves at the ranges of this experiment.

The travel times calculated for a variety of laterally homogeneous, layered velocity structures have been compared with the travel time data. A ray tracing program allowed forward modeling of the arrivals. Comparison of the stacked record section with WKBJ synthetic seismograms [*Chapman*, 1978] has also been carried out for each model. All of the travel times calculated from the models discussed below fit the travel time data. For a preferred model the WKBJ synthetic seismograms provide a good fit to the observed DOBH records (Figure 14) as well.

Velocity model 1 (Figure 15a) consists of six layers, each characterized by a linear velocity gradient. A thin (0.2-km thick) surface layer with a high velocity

gradient (6.3 s^{-1}) overlies a 1-km thick layer with a lesser gradient (0.6 s^{-1}). A third layer 0.8-km thick has a velocity of 5 km/s and a very low gradient. A transitional fourth layer, 0.4-km thick, has a gradient of 4.7 s^{-1}. A fifth layer 0.5-km thick has a velocity of about 6.5 km/s and a gradient of 0.2 s^{-1}. Mantle velocity (7.9 km/s) is reached at a depth of about 3 km; the upper mantle velocity gradient is 0.03 s^{-1}.

The travel times and WKBJ synthetic seismograms for model 1 are shown in Figures 15b and 15c. Selected ray paths for this model are displayed in Figure 16. The high velocity gradient upper layer results in an amplitude high at short ranges (1-3.5 km). Two triplications resulting from regions of high velocity gradient in the lower crust are together responsible for the high-amplitude arrivals having a phase velocity of about 6.5 km/s. The lower of these two regions is represented as a first-order discontinuity in the model (Figure 15a), so the prominent arrivals at 7-11 km range associated with this discontinuity are sub-critical Moho reflections. Refractions from a high-gradient Moho transition zone of finite depth extent would provide a comparable amplitude-range pattern. The travel time curves for this model fit the observed travel times fairly well (Figure 15b) and the WKBJ synthetics (Figure 15c) match the general amplitude character of the stacked record section (Figure 14). For these reasons, model 1 is the preferred model.

Velocity model 2 (Figure 17a) is included to support the inference from model 1 that upper mantle velocities are required at a depth of about 3 km in order to satisify both the travel time and the amplitude data. Velocity in the first

five layers of model 2 are the same as in model 1. Only the lowermost layer differs. In model 2 there is no first-order discontinuity at the base of the crust, but rather a 3-km-thick layer with a gradient of 0.017 s^{-1}. Mantle velocity is reached at a depth of 6 km.

The amplitude pattern indicated by the WKBJ synthetics (Figure 17b) is not as good a fit to the data as model 1. Not only are the amplitudes too low for the second refracted branch (7-12 km range), but the apparent phase velocity at the triplication in the synthetics is less than the phase velocity of the observed data (Figure 14). The triplication caused by a single high velocity gradient in the lower crust is not adequate to match the observed amplitude-range pattern.

Velocity model 3 (Figure 18a) is included to support the inference from model 1 that two regions of high velocity gradient are required in the lower crust, i.e., that two triplications interact to satisify the phase velocity and amplitudes observed on the record section at 7-12 km range. In the uppermost 1.2 km, model 3 is identical to models 1 and 2. In model 3, however, the 0.6 s^{-1} gradient layer continues to a first order discontinuity at a depth of about 2.3 km. The underlying layer has a velocity gradient similar to the that of second layer; upper mantle velocity is reached at a depth of about 7.5 km.

The high phase velocity arrivals at range 6.5-12 km in the observed record station are not modeled adequately by model 3. The high amplitudes are shifted to too large a range and the slope of the branch is 5 km/s, too low to fit our data.

Because of the water depth (3800 m), the data from this experiment do not constrain the velocity structure of the uppermost 0.5 km of oceanic crust. Without

a source and receiver on the sea floor, shallow crustal refractions are lost in the water wave. A very low velocity upper crust can be inferred, however, by the absence of S-waves in our record section. If the thickness of the uppermost layer of low velocity is greater than half an S-wave wavelength, then P-to-S conversion at the seafloor-water interface will be inefficient [*White and Stephen,* 1980]; in model 1 the S-wave wavelength at 9 Hz is about 200 m in the uppermost crust, comparable to the thickness of the surficial low-velocity layer.

STRUCTURAL COMPARISON OF THE MEDIAN RIDGE WITH ADJACENT REGIONS

The preferred velocity model for the median ridge (Figure 15a) may be regarded as consisting of 2-3 crustal layers separated by transition zones of high velocity gradients. One might associate the 2-km-thick region having velocity near 5 km/s with oceanic layer 2 and the 0.5-km-thick layer having velocity near 6.5 km/s with a highly thinned oceanic layer 3. The velocities in the median ridge model are somewhat lower than typical for these layers in "normal" oceanic crust, however, and the small crustal thickness and thin-to-absent layer 3 are more typical of the crustal structure found elsewhere in large-offset, slow-slipping fracture zones [*Cormier et al.*, 1984; *White et al.*, 1984].

We may demonstrate this association more directly by comparing record sections and inferred crustal models for the median ridge with those from two separate experiments conducted in the Kane Fracture Zone region. The first is the air-gun refraction line (experiment 2, OBH) of *Cormier et al.* [1984] shot along the fracture zone trough 50 km to the east of the eastern ridge-transform intersection (Figure 19). The second is the "H" experiment of *White and Purdy* [1983] (Figure 20), a series of air-gun refraction lines conducted to determine the upper crustal structure and its variability within a small (10km by 15 km) area of 10 My-old crust located 50 km north of the eastern ridge-transform intersection of the Kane (Figure 2). This age would be similar to that of the median ridge if the ridge formed at the western ridge-transform intersection. Refracted arrivals from one of the air-gun lines of the "H" experiment were repicked and water-path

corrected to be consistent with the results from the median ridge.

A comparison of the first-arrival travel times, corrected for topography, from the three experiments is shown in Figure 21. It is apparent that the refracted arrivals at 2-4 km range along this one particular line of the "H" experiment have a phase velocity that is slower than the corresponding arrivals from the median ridge or fracture zone trough. A comparison of velocity-depth functions from all six lines of the "H" experiment with the preferred model for the median ridge (Figure 22), however, indicates that the shallow structure of the median ridge falls within the range in upper crustal structure found for 10-My-old seafloor.

The most striking comparison is between the median ridge and the fracture zone trough. In particular, the two record sections bear a remarkable similarity (compare Figures 19 and 14). The principal difference is at short range, where shallow crustal refractions turned from the uppermost 1.5 km are visible on Figure 14 but not on Figure 19. This may be due to the fact that the water depth along the trough (4.5-5 km) was greater than the depth of the median ridge. The shallow refracted arrivals, by this reasoning, are obscured by the direct water wave for the trough profile (Figure 19). Beyond this difference, amplitude patterns at 7-12 km range are a good match between the two profiles, as are the phase velocities of the principal arrival. Not surprisingly, the velocity structure determined by *Cormier et al.* [1984] from the data is also similar to the median ridge model (Figure 22).

A slight difference however, between the median ridge velocity structure and the structure of *Cormier et al.* [1984] may be seen observed in the travel

times at 7-10 km range (Figure 21) and in the velocity structures (Figure 22). This difference may be due to variations in composition or fracture porosity in the lower crust of the fracture zone trough or it simply may be an expression of the greater age of the crust at the site of the *Cormier et al.* [1984] air gun experiment.

A comparison was made between the mantle (two-way) delay time for the median ridge and the mantle delay time obtained by *Cormier et al.* [1984] along the fracture zone trough south of the median ridge. The mantle delay time in the trough (1.8 s) is approximately twice that of the median ridge (0.87 s), indicating that considerably thicker crust underlies the fracture zone adjacent to the southern boundary of the median ridge.

EVALUATION OF MODELS FOR MEDIAN RIDGES

The results of the above analysis of the refraction experiment may now be compared with the predictions of the various hypotheses for the formation of fracture zone median ridges. We regard the following inferences about median ridge structure as particularly noteworthy:

(1) Upper mantle velocities are found at a depth of 3 km beneath the Kane Fracture Zone median ridge. The record section from the median ridge bears a close resemblance to the record section from the aseismic portion of the fracture zone trough 150 km east of the ridge-transform intersection [*Cormier et al.*, 1984].

(2) Mantle delay time experiments in the aseismic fracture zone limb [*Cormier et al.,* 1984] reveal that the zone of pronounced thinning of the crust at the fracture zone is only about 10 km wide.

(3) In contrast to the aseismic fracture zone limb the axis of the transform trough to the south of the median ridge is underlain by crust of nearly normal (6-7 km) thickness [*Cormier et al.,* 1984].

(4) The shallow velocity structure of the median ridge and of the trough of the aseismic fracture zone limb [*Cormier et al.,* 1984] both fall within the bounds of nearby 'normal' oceanic crust [*Purdy and White,* 1983].

(5) The proximity of the median ridge to the axis of the transform valley and to the proposed location of the PTDZ [*Garfunkel*, 1986; *Pockalny et al.*, 1987] suggest that the median ridge is close to or within the transform fault zone.

(6) No median ridges are revealed in numerous wide beam echo sounder

crossings of the aseismic limb of the Kane Fracture Zone to a distance of at least 200 km from the eastern ridge-transform intersection.

Of the mantle diapir models for median ridge formation (Figures 9 and 10), models in which the thickness of layers with crustal velocities beneath the median ridge is comparable to (Figure 10b and d) or greater than (Figure 10a) that beneath the surrounding crust can be excluded. The median ridge is underlain by no more than 3 km of material with crustal velocities (Figure 15), while the fracture zone trough immediately adjacent is underlain by crust 6-7 km thick [*Cormier et al.*, 1984]. At face value, this argument would also rule out the model in Figure 10c in which thinned fracture zone crust surrounded by normal oceanic crust has been uplifted by an underlying layer at least 3-4 km thick of serpentinized mantle. One means by which this model might still be consistent with the seismic data is if the uppermost portion of the serpentine layer, immediately beneath the crust, were at most modestly altered and thus preserved mantle velocities while the lower portions had a much greater degree of alteration. The refraction experiment did not extend to sufficient range to sample the depths (> 3 km) necessary to test this conjecture. The model should be considered speculative, however, as a decrease in the degree of serpentinization with depth would be a more natural consequence of alteration by circulation of seawater through fissures and faults.

Models involving uplift or flexure by the action of compressional stress acting across the fracture zone cannot be strictly excluded by the seismic data. Nonetheless such models cannot account for the observation that the crust of the

median ridge is *thinner* than the crust of the adjacent transform trough. Thrust faulting would lead to crustal *thickening,* while flexure of the elastic lithosphere would, to first order, leave crustal thickness unmodified. Also, as noted earlier, there is no evidence from earthquake mechanisms or plate kinematic reconstructions for a significant component of compressive stress acting across the Kane transform. If there is any significant normal stress across the transform, it is more likely to be extensional [*Garfunkel,* 1986].

Models for median ridge formation involving intratransform volcanic construction or formation of new crust within a leaky transform are similarly difficult to rule out. Nonetheless these models do not provide a natural explanation for why the crust of the median ridge should be thinner than that of surrounding terrain; simple volcanic construction should yield thicker crust beneath the construct once volcanism was complete. As noted above, limited sampling of the median ridge indicates basaltic material but only highly altered rocks suggestive of an extended time interval since the most recent volcanic episode.

Models involving lateral heat transport do not provide a straightforward explanation for median ridge formation because the median ridge is narrower than the characteristic width of most lithospheric thermal anomalies and because the most likely sources of heat (the spreading ridge axes) are at considerable distance from the median ridge along most of its length. In addition, lateral heat transport cannot account for thinnner crust beneath the median ridge than beneath adjacent portions of the fracture zone.

Thus, none of the simple hypotheses for median ridge formation provide altogether acceptable explanations of the structure. Any isostatic model (e.g., Figure 10) faces the obstacle that the ridge stands higher, but is underlain by thinner crust, than surrounding terrain. Non-isostatic models (e.g., involving the effects of horizontal lithospheric stress or sub-lithospheric processes) are possible but are ill-specified and difficult to test.

A number of additional experiments would help to remove the ambiguities and uncertainties that have prevented a more definitive test of competing models. A gravity survey of the transform at a horizontal resolution sufficient to resolve the median ridge should indicate the nature of isostatic compensation across the transform. Additional refraction data extended to greater range than in this experiment would help define the P-wave velocity structure at depths greater than 3 km. Measurement of S-wave velocity structure, using either natural or artificial sources, would provide an important test of the presence of serpentine. Further sampling of the median ridge by dredging, submersible, and drilling will help to define the nature of the surface and shallow crustal material making up the ridge. Additional geological observations by submersible or deep-towed imaging systems should help to constrain the principal fault systems along and adjacent to the median ridge. Careful heat flow measurements across the transform might reveal or rule out the possibility of a thermal component of the relief. Finally, detailed microearthquake experiments within the transform should help to define the locus of the PTDZ, the mechanisms of earthquakes along the active fault trace, and their relationship to the median ridge.

CONCLUSIONS

A refraction study of the median ridge of the Kane transform was conducted with an air gun source and a seafloor receiver. Analysis of first-arrival travel times and modelling the amplitudes with a WKBJ method permit the P wave velocity beneath the ridge to be reasonably well-constrained. The crust beneath the median ridge appears to be about 3 km thick. The upper kilometer of the structure falls within the bounds of nearby 'normal' oceanic crust [*White and Purdy*, 1983]. The overall structure is similar to that found by *Cormier et al.* [1984] along the fracture zone trough 150 km east of the ridge-axis intersection. These comparisons suggest that the median ridge is composed of thinned fracture-zone crust that, through some process, has been uplifted.

It appears that none of the simple models for median ridge formation are altogether consistent with the seismic data. Most models requiring isostatic equilibrium are suspect because thin crust of the median ridge is flanked by thicker crust in the adjacent transform trough [*Cormier et al.*, 1984]. Models involving compressive stress or intratransform volcanism are possible, but these models do not account readily for median ridge crust that is thinner than that of surrounding terrain and, in addition, supporting evidence for these models (e.g., earthquake mechanisms, fresh basalt recovered from the median ridge) is lacking.

The absence of any ridge-parallel fabric on the median ridge of the Kane transform and the extremely thin crust suggest that the median ridge is not formed by conventional accretionary processes. It is not clear if the median ridge if

currently part of the African plate or the North American plate, or even whether the ridge has always resided on the same plate (i.e., the same side of the PTDZ). The apparent absence of a median ridge outside the transform zone could be taken to mean that generation of a median ridge structure is episodic, that an element of dynamic support within the transform is required to maintain the relief, or that the ridge structure is removed due by complex tectonic, thermal or volcanic processes operating at the nodal deeps. The common occurrence of median ridges within other large-offset fracture zones would seem to rule out the first possibility.

The data presented in this thesis do not resolve many of the outstanding questions on the origin or evolution of fracture zones. It is hoped that the added constraints imposed by the results of the refraction analysis will nonetheless aid in further investigation.

References

Bonatti, E., Serpentine protrusions in the oceanic crust, *Earth Planet. Sci. Lett., 32,* 107-113, 1976.

Bonatti, E., Vertical tectonism in oceanic fracture zones, *Earth Planet. Sci. Lett., 37,* 369-379, 1978.

Bonatti, E., and P. R. Hamlyn, Mantle uplifted blocks in the western Indian Ocean, *Science, 201,* 249-251, 1978.

Bonatti, E., and J. Honnorez, Sections of the Earth's crust in the equatorial Atlantic, *J. Geophys. Res., 81,* 4104-4116, 1976.

Bonatti, E., J. Honnorez, P. Kirst, and F. Radicati, Metagabbros from the Mid-Atlantic Ridge at 6°N: Contact-hydrothermal-dynamic metamorphism beneath the axial valley, *J. Geol., 83,* 61-78, 1975.

Bonatti, E., G. Ottonello, and P. R. Hamlyn, Peridotites from the island of Zabargad (St. John), Red Sea: Petrology and geochemistry, *J. Geophys. Res., 91,* 599-631, 1986.

Calvert, A. J., and C. G. Potts, Seismic evidence for hydrothermally altered upper mantle beneath old crust in the Tydeman Fracture Zone, *Earth Planet. Sci. Lett., 75,* 439-449, 1985.

Chapman, C.H., A new method for computing synthetic seismograms, *Geophys. J. R. Astron. Soc., 54,* 481-518, 1978.

Christensen, N. I., Elasticity of ultrabasic rocks, *J. Geophys. Res., 71,* 5921-5931, 1966.

Christensen, N. I., The abundance of serpentinites in the oceanic crust, *J. Geol., 80,* 709-719, 1972.

Coleman, R. G., Petrological and geophysical nature of serpentinites, *Bull. Geol. Soc. Amer., 82,* 897-918, 1971.

Collette, B. J., Thermal contraction joints in a spreading seafloor as origin of fracture zones, *Nature, 251,* 299-300, 1974.

Collette, B. J., A. P. Slootweg, J. Verhoef, and W. R. Roest, Geophysical investigations of the floor of the Atlantic Ocean between 10° and 38° (Kroonvlag-project), *Proc. Koninklijke Nederlandse Akademie van*

Wetenschappen, Series C, *87*, 1-76, 1984.

Cormier, M. H., R. S. Detrick, and G. M. Purdy, Anomously thin crust at oceanic fracture zones: New seismic constraints from the Kane Fracture Zone, *J. Geophys. Res., 89,* 10249-10266, 1984.

CYAMEX Scientific team and L. Pastouret, Submersible structural study of Tamayo transform fault, East Pacific Rise, 23°N (Project RITA), *Mar. Geophys. Res., 4,* 381-402, 1981.

Detrick, R. S., and G. M. Purdy, The crustal structure of the Kane Fracture Zone from seismic refraction studies, *J. Geophys. Res., 85*, 3759-3777, 1980.

Detrick, R. S., M. H. Cormier, R. Prince, and D. W. Forsyth, Seismic constraints on the crustal structure within the Vema Fracture Zone, *J. Geophys. Res., 87,* 10599-10612, 1982.

Dick, H.B.J., Petrologic variability of the oceanic crust and uppermost mantle, U.S.G.S. Circular, *Geophysics and Petrology of the Deep Crust and Mantle,* submitted, 1986.

Engel, C. G., and R. L. Fisher, Granitic to ultramafic rock complexes of the Indian Ocean ridge system, western Indian Ocean, *Bull. Geol. Soc. Amer., 86,* 1553-1578, 1975.

Fox, P. J., and D. G. Gallo, A tectonic model for ridge-transform-ridge plate boundaries: Implications for the structure of oceanic lithosphere, *Tectonophysics, 104,* 205-242, 1984.

Fox, P. J., W. C. Pitman III, and F. Shepard, Crustal plates in the Central Atlantic: Evidence for at least two poles of rotation, *Science, 165,* 487-489, 1969.

Fox, P. J., E. Schreiber, and J. J. Peterson, The geology of the oceanic crust: Compressional velocities of oceanic rocks, *J. Geophys. Res., 78,* 5155-5172, 1973.

Fox, P. J., E. Schreiber, H. Rowlett, and K. McCamy, The geology of the Oceanographer Fracture Zone: A model for fracture zones, *J. Geophys. Res., 81*, 4117-4128, 1976.

Francheteau, J., P. Choukroune, R. Hekinian, X. Le Pichon, and D. Needham, Oceanic fracture zones do not provide deep sections into the crust, *Can. J.*

Earth Sci., 13, 1223-1235, 1976.

Francis, T. J. G., Serpentinization faults and their role in the tectonics of slow spreading ridges, *J. Geophys. Res., 86,* 11616-11622, 1981.

Gallo, D. G., Fox, P. J., and K. C. Macdonald, A Sea Beam investigation of the Clipperton transform fault: The morphotectonic expression of a fast slipping transform boundary, *J. Geophys. Res., 91*, 3455-3467, 1986.

Garfunkel, Z., Review of oceanic transform activity and development, *J. Geol. Soc. Lond., 143*, 775-784, 1986.

Gregory, R. T., and H. P. Taylor, Jr., An oxygen isotope profile in a section of Cretaceous ocean crust, Samail Ophiolite, Oman: Evidence for $\delta^{18}O$ buffering of the oceans by deep (>5 km) seawater-hydrothermal circulation of mid-ocean ridges, *J. Geophys. Res., 86*, 2737-2755, 1981.

Hebert, R., D. Bideau, and R. Hekinian, Ultramafic and mafic rocks from the Garrett transform fault near 13°30'S on the East Pacific Rise: Igneous petrology, *Earth Planet. Sci. Lett., 65*, 107-125, 1983.

Karson, J. A., and H. J. B. Dick, Tectonics of ridge-transform-ridge intersections at the Kane Fracture Zone, *Mar. Geophys. Res., 6,* 51-98, 1983.

Karson, J. A., J. R. Brown, and A. T. Winters, Seafloor spreading in the MARK area (abstract), *Eos. Trans. Amer. Geophys. Un., 67*, 1213, 1986.

Kastens, K. A., K. C. Macdonald, S. P. Miller, and P. J. Fox, Deep tow studies of the Vema Fracture Zone, 2, Evidence for tectonism and bottom currents in the sediments of the transform valley floor, *J. Geophys. Res., 91*, 3355-3367, 1986.

Kennett, B. L. N., and J. A. Orcutt, A comparison of travel time inversions for marine refraction profiles, *J. Geophys. Res., 81,* 4061-4070, 1976.

Kingma, J. T., Possible origin of piercement structures, local unconformities and secondary basins in the eastern geosyncline, New Zealand, *N. Z. J. Geol. Geophys., 1,* 269-274, 1958.

Koelsch, D., K. Peal, and G.M. Purdy, W.H.O.I. digital ocean bottom hydrophone instrument, *W.H.O.I. Technical Report 82-30*, 1982.

Lonsdale, P. Near-bottom reconnaissance of a fast-slipping transform fault zone

at the Pacific-Nazca plate boundary, *J. Geol., 86*, 451-472, 1978.

Louden, K. E., and D. W. Forsyth, Crustal structure and isostatic compensation near the Kane Fracture Zone from topography and gravity measurements, 1, Spectral analysis approach, *Geophys. J. R. Astron. Soc., 68,* 725-750, 1982.

Louden, K. E., R. S. White, C. G. Potts, and D. W. Forsyth, Structure and seismotectonics of the Vema Fracture Zone, Atlantic Ocean, *J. Geol. Soc., 143*, 795-805, 1986.

Ludwig, W. J., and P. D. Rabinowitz, Structure of the Vema Fracture Zone, *Mar. Geol., 35,* 99-110, 1980.

Macdonald, K. C., J. C. D. Castillo, S. Miller, P. J. Fox, K. Kastens, and E. Bonatti, Deep-tow studies of the Vema Fracture Zone, 1, Tectonics of a major slow-slipping transform fault and its intersection with the Mid-Atlantic Ridge, *J. Geophys. Res., 91,* 3334-3354, 1986.

Mann, P., M. R. Hempton, D. C. Bradley, and K. Burke, Development of pull-apart basins, *J. Geol., 91*, 529-554, 1983.

Melson, W. G., E. Jarosevich, R. Cifelle, and G. Thompson, St. Peter and St. Paul rocks: a high temperature mantle-derived intrusion, *Science, 155*, 1532-1535, 1967.

Menard, H. W., and T. Atwater, Changes in direction of sea floor spreading, *Nature, 219,* 463-467, 1968.

Menard, H. W., and T. Atwater, Origin of fracture zone topography, *Nature, 222,* 1037-1041, 1969.

Minster, J. B., and T. H. Jordan, Present-day plate motions, *J. Geophys. Res., 83,* 5331-5354, 1978.

Michael, P. J., and E. Bonatti, Peridotite composition from the North Atlantic: Regional and tectonic variations and implications for partial melting, *Earth Planet. Sci. Lett., 73,* 91-104, 1985.

OTTER (Oceanographer Tectonic Research Team: J. A. Karson, P. J. Fox, H. Sloan, K. T. Crane, W. S. F. Kidd, E. Bonatti, J. B. Stroup, D. J. Fornari, D. Elthon, P. Hamlyn, J. F. Casey, D. G. Gallo, D. Needham, and R. Sartori), The geology of the Oceanographer transform: The ridge-transform intersection,

Mar. Geophys. Res., 6, 109-141, 1984.

OTTER (Oceanographer Tectonic Research Team: P. J. Fox, R. J. Moody, J. A. Karson, K. T. Crane, W. S. F. Kidd, E. Bonatti, J. B. Stroup, D. J. Fornari, D. Elthon, P. Hamlyn, J. F. Casey, D. G. Gallo, D. Needham, and R. Sartori), The geology of the Oceanographer transform: The transform domain, *Mar. Geophys. Res., 7,* 329-358, 1985.

Parmentier E. M., and W. F. Haxby, Thermal stresses in the oceanic lithosphere: Evidence from geoid anomalies at fracture zones, *J. Geophys. Res., 91,* 7193-7204, 1986.

Phipps Morgan, J., and D. W. Forsyth, 3-D flow and temperature perturbations due to a transform offset: Effects on oceanic crustal and upper mantle structure, *J. Geophys. Res.,* in press, 1987.

Pockalny, R. A., R. S. Detrick, and P. J. Fox, The morphology and tectonics of the Kane transform from Sea Beam bathymetry data, *J. Geophys. Res.,* in press, 1987.

Potts, C. G., R. S. White, K. E. Louden, Crustal structure of Alantic fracture zones, 2, The Vema Fracture Zone and transverse ridge, *Geophys. J. R. Astron. Soc., 86,* 491-513, 1986.

Purdy, G. M., The correction for the travel time effects of seafloor topography in the interpretation of marine seismic data, *J. Geophys. Res., 87,* 8389-8396, 1982.

Purdy, G. M., and R. S. Detrick, The crustal structure of the Mid-Atlantic Ridge at 23°N from seismic refraction studies, *J. Geophys. Res., 91,* 3739-3762, 1986.

Purdy, G. M., P. D. Rabinowitz, and J. J. A. Velterop, The Kane Fracture Zone in the central Atlantic Ocean, *Earth Planet. Sci. Lett., 45,* 429-434, 1979.

Rabinowitz, P. D., and G. M. Purdy, The Kane Fracture Zone in the western central Atlantic Ocean, *Earth Planet. Sci. Lett., 33,* 21-26, 1976.

Rona, P. A., L. Widenfalk, and K. Boström, Serpentinized ultramafics and hydrothermal activity at the Mid-Atlantic Ridge crest near 15°N, *J. Geophys. Res., 92,* 1417-1427, 1987.

Sandwell, D. T., Thermomechanical evolution of oceanic fracture zones, *J.*

Geophys. Res., 89, 11401-11413, 1984.

Sandwell, D. T., and G. Schubert, Lithospheric flexure at fracture zones, *J. Geophys. Res., 87,* 4657-4667, 1982.

Schouten, H., and K. D. Klitgord, The memory of the accreting plate boundary and the continuity of fracture zones, *Earth Planet. Sci. Lett., 59,* 255-266, 1982.

Schouten, H., K. D. Klitgord, and J. A. Whithead, Segmentation of mid-ocean ridges, *Nature, 317,* 225-229, 1985.

Schouten, H., G.M. Purdy, and P.R. Rabinowitz, History of the Kane Fracture Zone
(abstract), *Eos Trans. Amer. Geophys. Un., 60,* 394, 1979.

Searle, R. C., Side-scan sonar studies of North Atlantic fracture zones, *J. Geol. Soc. Lond., 136,* 283-294, 1979.

Searle, R. C., Multiple, closely-spaced transform faults in fast-slipping fracture zones, *Geology, 11,* 607-610, 1983.

Searle, R. C., GLORIA investigations of oceanic fracture zones: Comparative study of the transform fault zone, *J. Geol. Soc. Lond., 143,* 743-756, 1986.

Segall, P., and D. D. Pollard, The mechanics of discontinuous faults, *J. Geophys. Res., 85,* 4337-4350, 1980.

Sinha, M. C., and K. E. Louden, The Oceanographer Fracture Zone, 1, Crustal structure from seismic refraction studies, *Geophys. J. R. Astron. Soc., 75,* 713-736, 1983.

Sykes, L. R., Mechanisms of earthquakes and nature of faulting on the Mid-Atlantic Ridge, *J. Geophys. Res., 72,* 2131-2153, 1967.

Thompson, G. and G. Melson, The petrology of oceanic crust across fracture zones in the Atlantic Ocean: Evidence of a new kind of seafloor spreading, *J. Geol., 80,* 526-538, 1972.

Tucholke, B. E., and H. Schouten, Global plate motion changes recorded in the Kane Fracture Zone (abstract), *Geol. Soc. Am. Abstr. Programs, 17,* 737, 1985.

Tucholke, B. E., and H. Schouten , The Kane Fracture Zone, *Mar. Geophys Res.,*

submitted, 1987.

Turcotte, D. L., Are transform faults thermal contraction cracks?, *J. Geophys. Res., 70,* 2573-2577, 1976.

White, R. S., Atlantic oceanic crust: Seismic structure of a slow spreading ridge, *Special Publication of the Geological Society, London, 16*, 34-44, 1983.

White, R. S., and G. M. Purdy, Crustal velocity structure on the flanks of the Mid-Atlantic Ridge at 24°N, *Geophys. J. R. Astron. Soc., 75*, 361-385, 1983.

White, R. S., and R.A. Stephen, Compressional to shear wave conversion in oceanic crust, *Geophys. J. R. Astron. Soc., 63,* 547-565, 1980.

White, R. S., R. S. Detrick, M. C. Sinha and M. H. Cormier, Anomalous seismic crustal structure of oceanic fracture zones, *Geophys. J. R. Astron. Soc., 79,* 779-798, 1984.

Whitehead, J. A., J. B. Dick, and H. Schouten, A mechanism for magmatic accretion under spreading centres, *Nature*, *312*, 146-148, 1984.

Whitmarsh, R. B., The Owen Basin off the south-east margin of Arabia and the evolution of the Owen Fracture Zone, *Geophys. J. R. Astron. Soc., 58,* 441-470, 1979.

Whitmarsh, R. B., and A. J. Calvert, Crustal structure of Atlantic fracture zones, 1, The Charlie Gibbs Fracture Zone, *Geophys. J. Roy. Astron. Soc., 85,* 107-138, 1986.

Wilson, J. T., A new class of faults and their bearing on continental drift, *Nature*, *73*, 1959-1982, 1965.

Figures

portion of the transform valley. From *Pockalny et al.* [1987].

Figure 7. Location of experiment (heavy stippled region) overlaid on simplified bathymetry and principal tectonic features as indicated by GLORIA images [*Searle*, 1986]. Heavy lines are principal lineaments in the transform zone; dotted lines are bathymetric contours, in km, from *Rabinowitz and Purdy* [1976]. Light stippled areas are depths less than 3 km. The DOBH location is indicated by a black triangle.

Figure 8. Cartoon view of the development of a serpentinized region along a transform fault leading to the formation of a median ridge. After *Francis* [1981]. From top to bottom: seawater flows down cracks along the fractured areas of the transform. A serpentinized region forms as the temperature drops. A diapir results from gravity instability, and a median ridge is formed.

Figure 9. Compressional velocity versus pressure for olivine-serpentine mixtures. The serpentine is from Burro Mountain, California. From *Christensen* [1966] and *Coleman* [1970].

Figure 10. Isostatic models of median ridge formation by serpentinization of a mantle layer. (a) Model involving a serpentine layer beneath an otherwise uniform section of thinned fracture-zone crust. (b) A serpentine diapir completely penetrating thinned fracture-zone crust. (c) A serpentine layer beneath a section of thinned fracture-zone crust surrounded by normal thickness crust on either side. (d) A model in which the fracture zone crust consists of altered mantle of

variable degrees of serpentinization; the median ridge is underlain by a nearly pure serpentine layer.

Figure 11. Cartoon view of a leaky transform. (a, b) In response to a change in the direction of spreading, a fracture zone opens as plates move apart in new directions. Volcanic material wells up into the opening. (c) The spreading ridges reorient themselves perpendicular to the new spreading direction. From *Menard and Atwater* [1968].

Figure 12. Air gun source signal obtained from a DOBH at a horizontal range of 1 km. The DOBH was anchored 1 km from the ocean bottom so that no sea floor interactions obscure the record.

Figure 13. Topographic profiles along the four tracks of the experiment.

Figure 14. Stacked record section from the four air-gun lines along the Kane Fracture Zone median ridge. A reduction velocity of 5 km/s has been assumed. Traces are truncated at the onset of the water wave.

Figure 15. (a) P-wave velocity model 1. (b) A comparison of travel times with the travel times of observed first arrivals. The observed travel times have been corrected for topography. (c) WKBJ synthetic seismograms for model 1.

Figure 16. Ray paths for model 1 (Figure 15). Rays differ by equal increments in the ray parameter. Two high gradient layers in the lower crust combine to provide high amplitudes at 7-11 km range.

Figure 17. (a) P-wave velocity model 2. (b) Predicted travel times compared with times of observed first arrivals. (c) WKBJ synthetic seismograms

for model 2.

Figure 18. (a) P-wave velocity model 3. (b) Predicted travel times compared with times of observed first arrivals. (c) WKBJ synthetic seismograms for model 3.

Figure 19. Record section from the air gun line along the eastern aseismic limb of the Kane Fracture Zone. Data are from experiment 2, OBH 3 [*Cormier et al.*, 1984]. The reduction velocity is 5 km/s. Note the strong similarity to Figure 14.

Figure 20. Record section from the air gun line of the "H" experiment in 10-My-old crust 20 km north of the Kane Fracture Zone. The reduction velocity is 5 km/s. From *White and Purdy* [1983].

Figure 21. Water-path-corrected travel times from this study (crosses) are compared with those from air gun line in the "H" experiment of *White and Purdy* [1983] (squares) and the fracture zone line of *Cormier et al.* [1984] (circles).

Figure 22. Preferred velocity structure (model) for the Kane Fracture Zone median ridge (dashed line) is compared with the range in velocity-depth functions from the "H" experiment [stippled region, *White and Purdy*, 1983] and the velocity structure of the aseismic limb of the Kane Fracture Zone [dash-dot line, *Cormier et al.*, 1984].

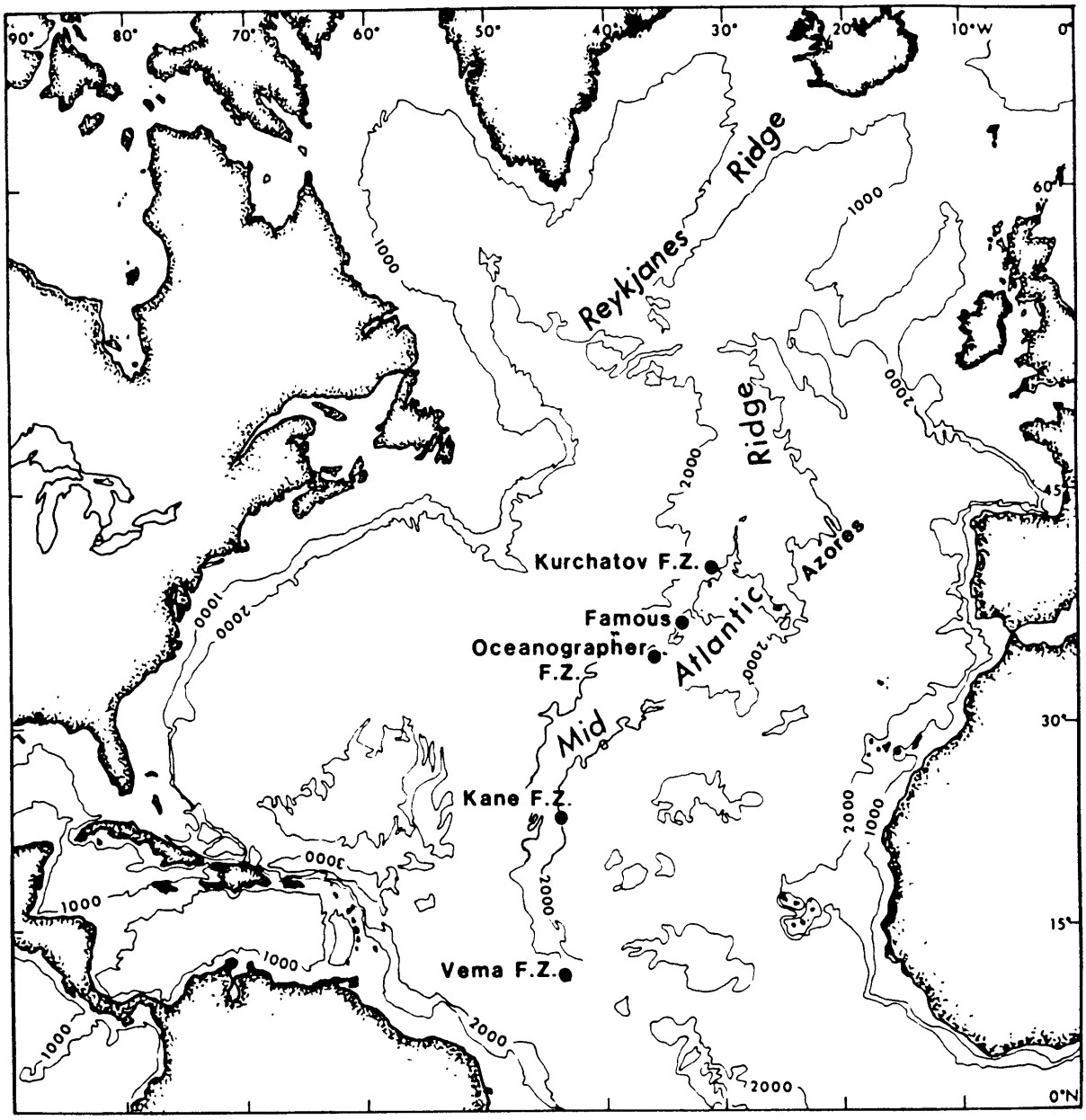
90°
80°
70°
60°
50°
40°
30°
20°
10°W
0°
60°
45°
30°
15°
0°N
Reykjanes Ridge
Mid Atlantic Ridge
Azores
Kurchatov F.Z.
Famous
Oceanographer F.Z.
Kane F.Z.
Vema F.Z.
1000
2000
3000

Figure 1

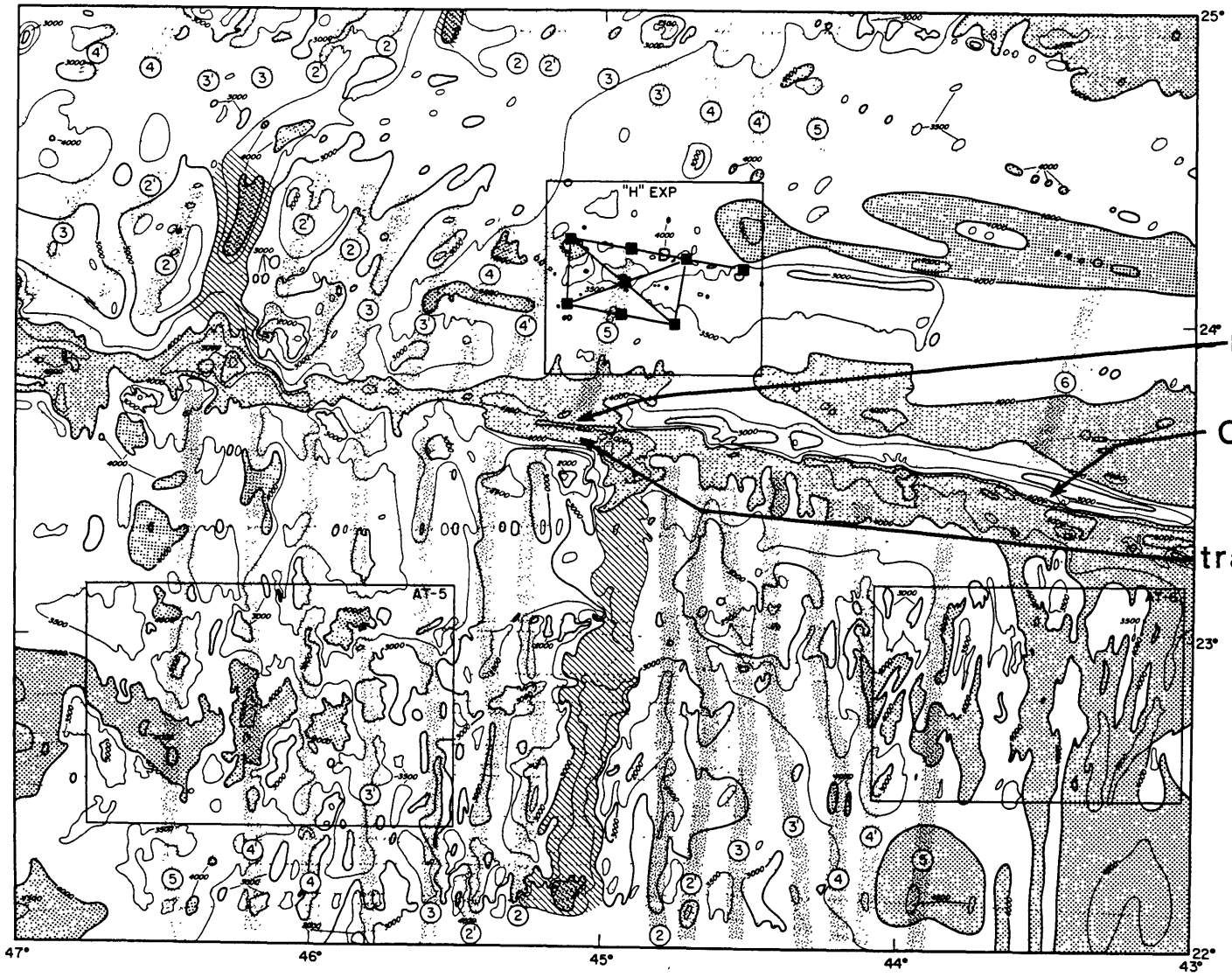
"H" EXP
AT-5
25°
24°
23°
22°
47°
46°
45°
44°
43°
median ridge
Cormier et al.,(1984)
air gun expt.
transform trough

Figure 2

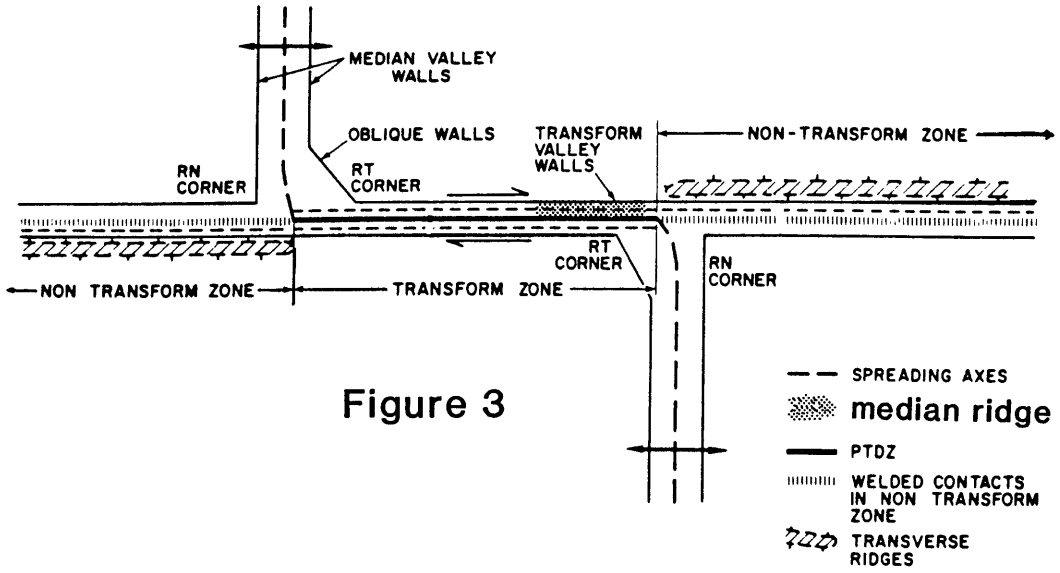

Figure 3

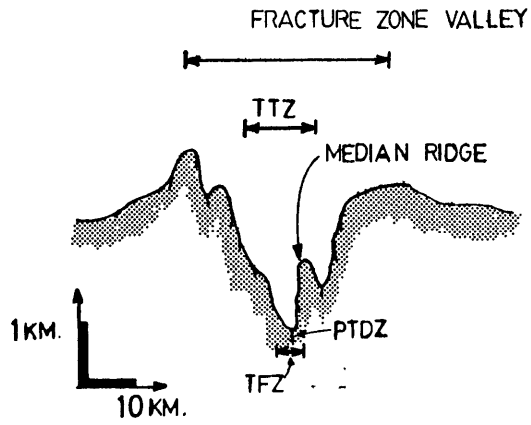

Figure 4

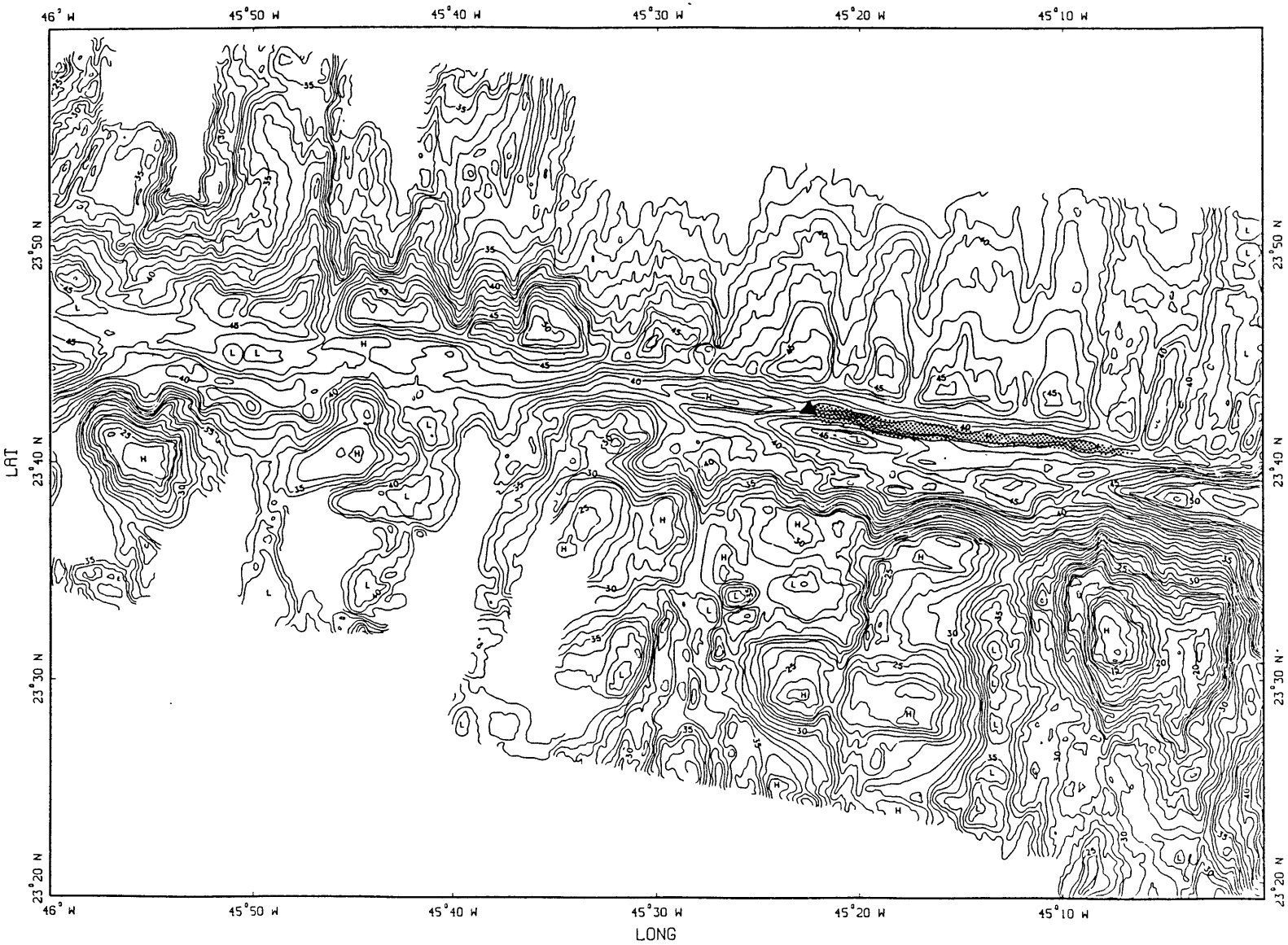
46° W
45°50 W
45°40 W
45°30 W
45°20 W
45°10 W
23°50 N
23°40 N
23°30 N
23°20 N
LAT
LONG

Figure 5

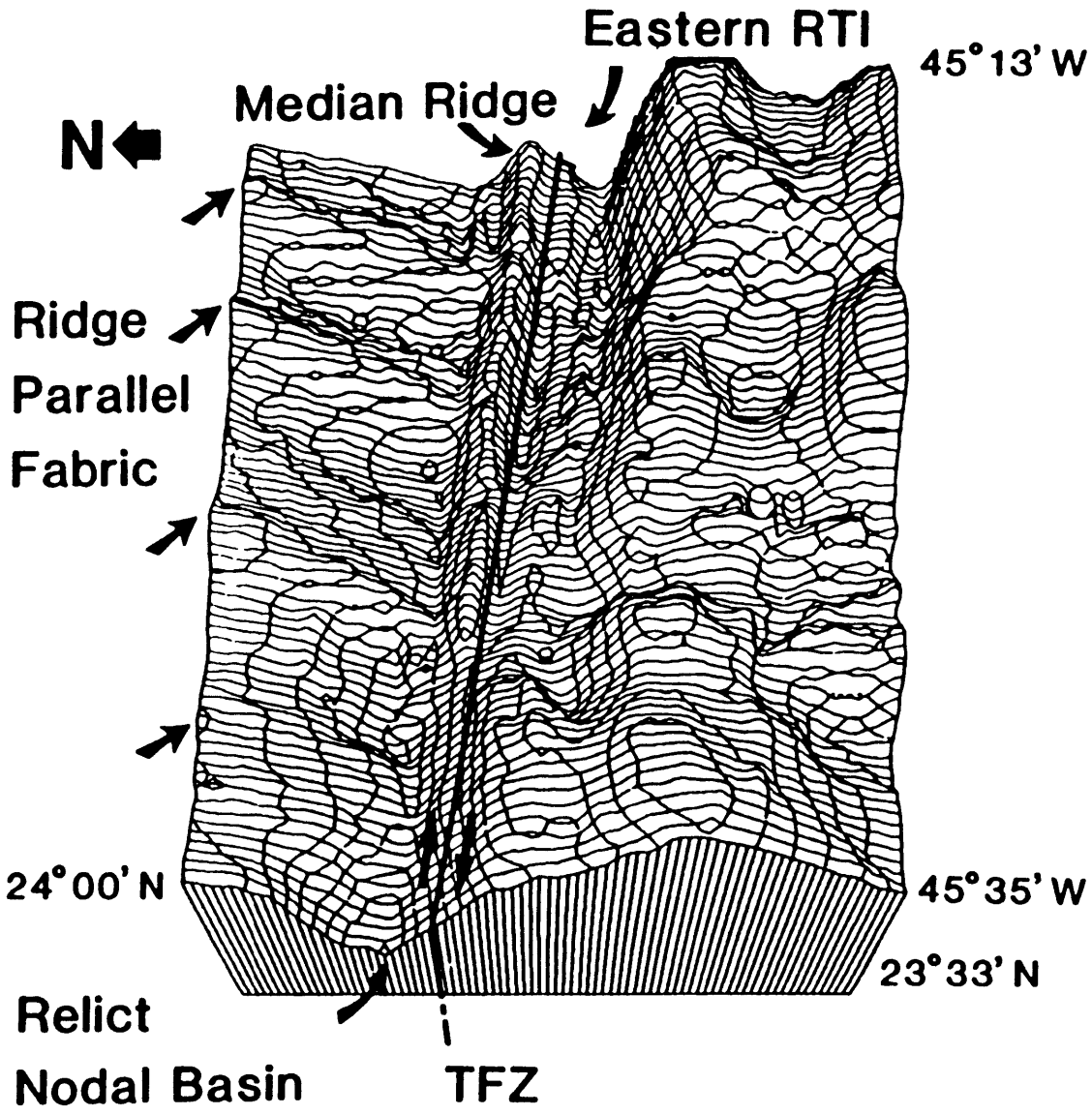
Eastern RTI
45°13' W
Median Ridge
N
Ridge
Parallel
Fabric
24°00' N
45°35' W
23°33' N
Relict
Nodal Basin
TFZ

Figure 6

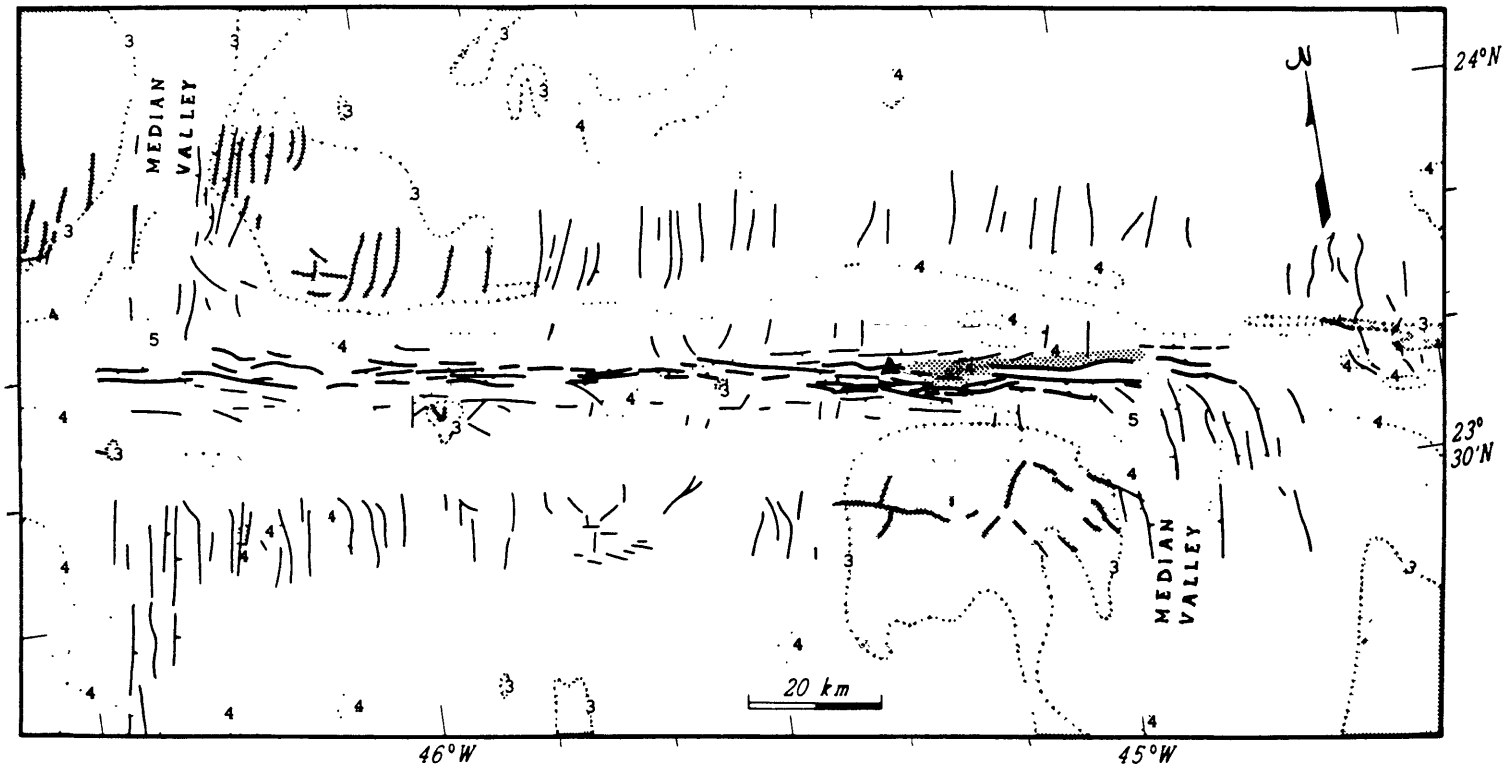

Figure 7

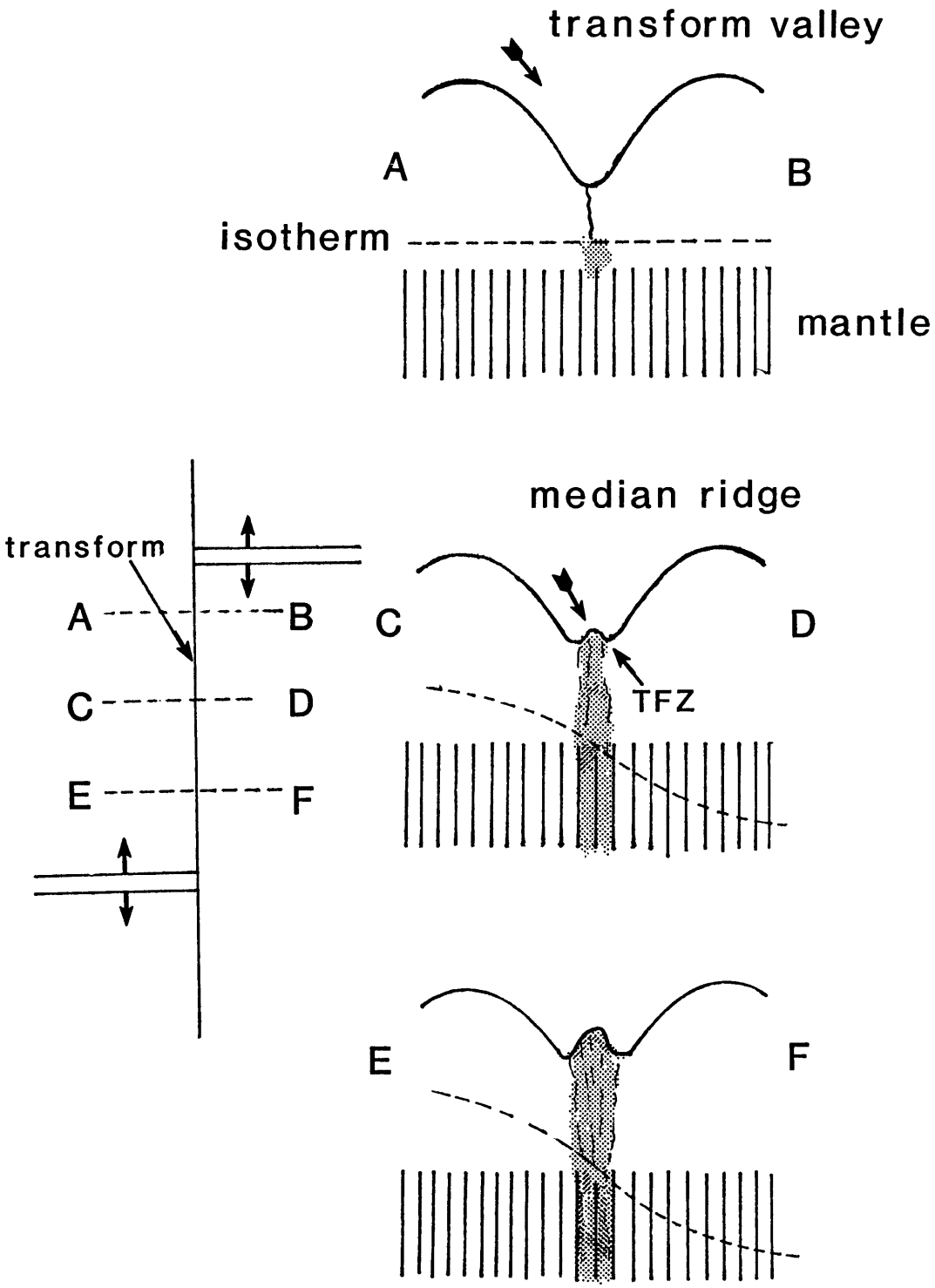
transform valley
A
B
isotherm
mantle
transform
A
B
C
D
E
F
median ridge
C
D
TFZ
E
F

Figure 8

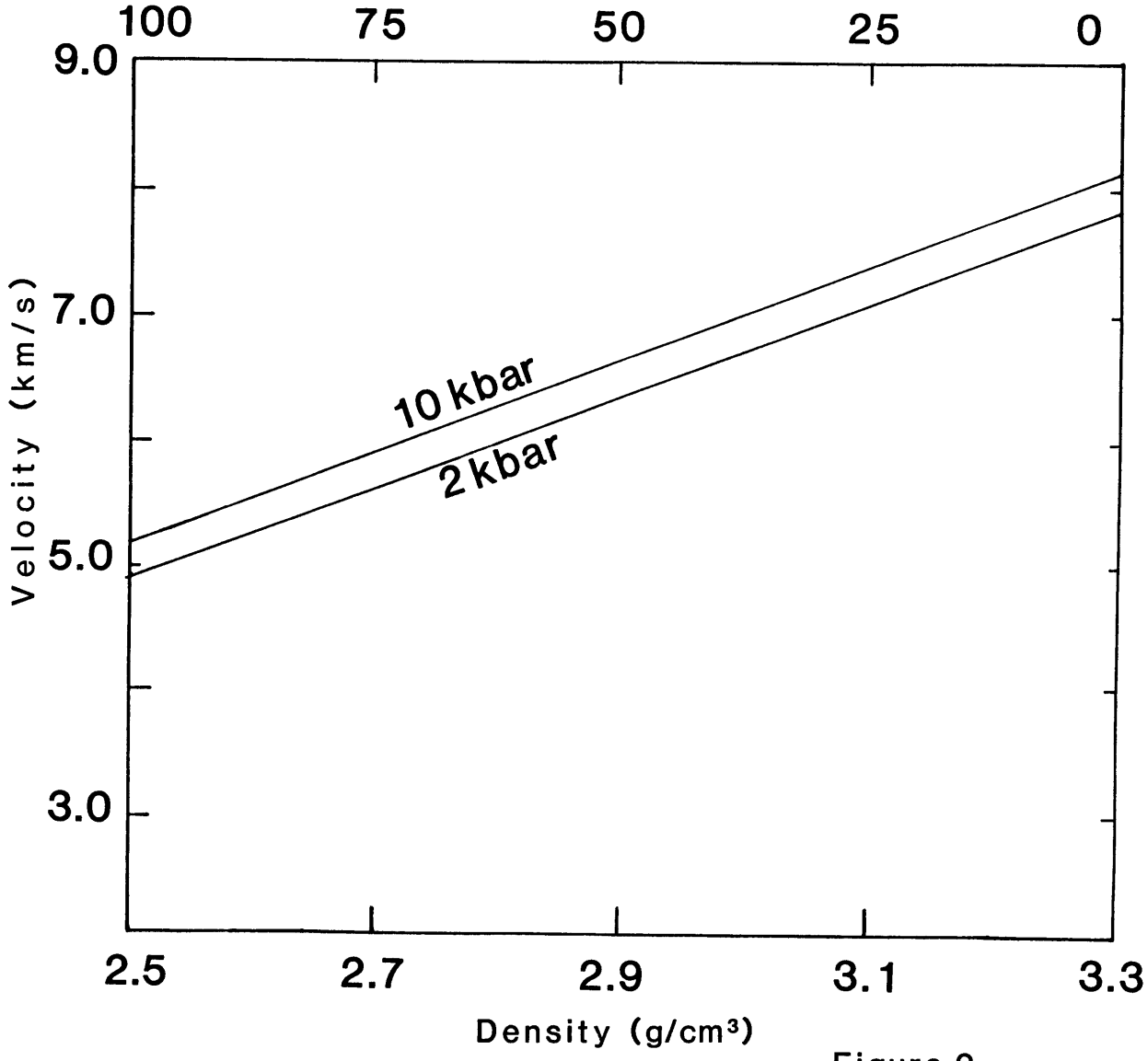
100
75
50
25
0
9.0
7.0
5.0
3.0
Velocity (km/s)
10 kbar
2 kbar
2.5
2.7
2.9
3.1
3.3
Density (g/cm³)

Figure 9

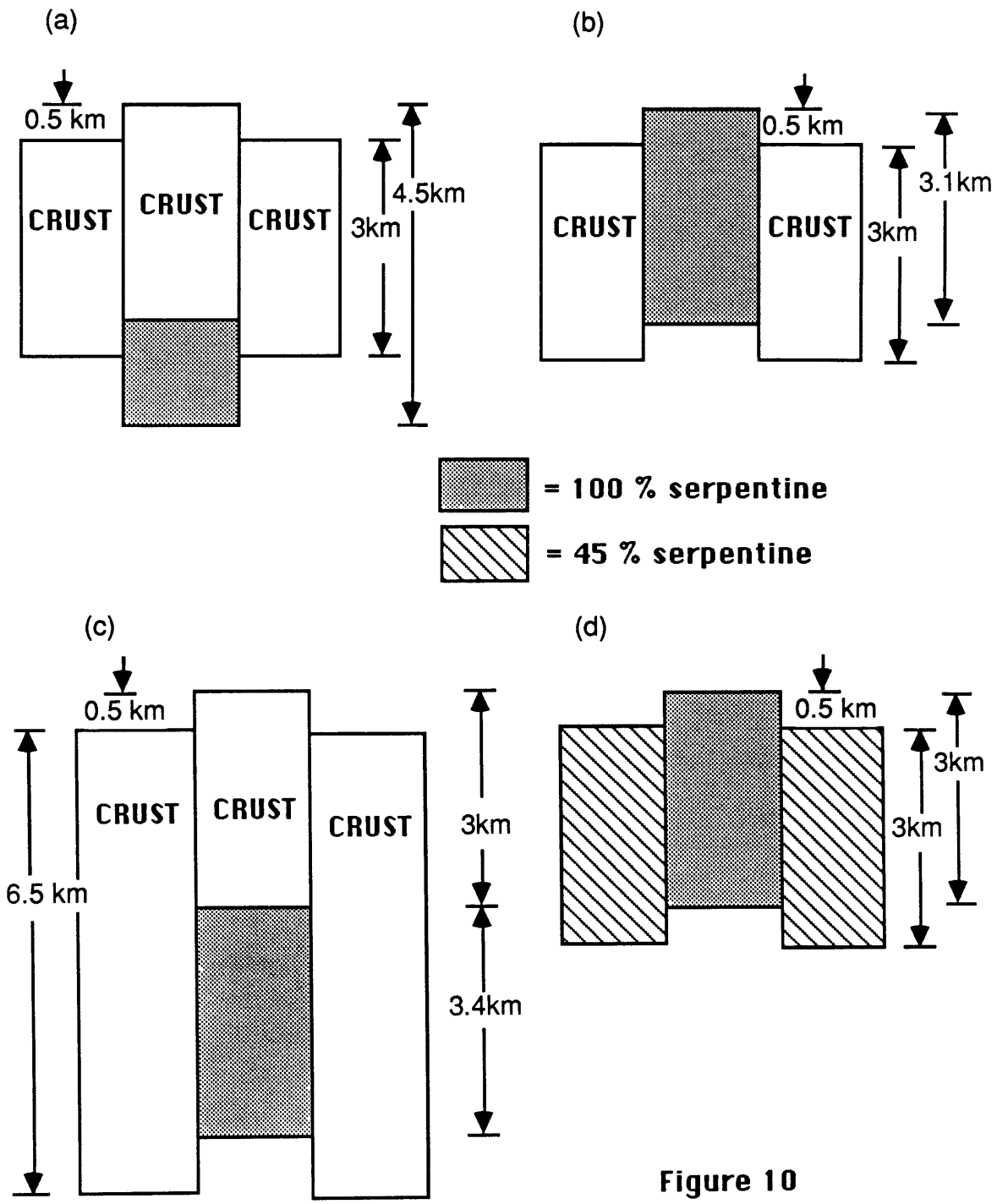
(a)
0.5 km
CRUST
CRUST
CRUST
3km
4.5km
(b)
0.5 km
CRUST
CRUST
3km
3.1km
= 100 % serpentine
= 45 % serpentine
(c)
0.5 km
CRUST
CRUST
CRUST
6.5 km
3km
3.4km
(d)
0.5 km
3km
3km

Figure 10

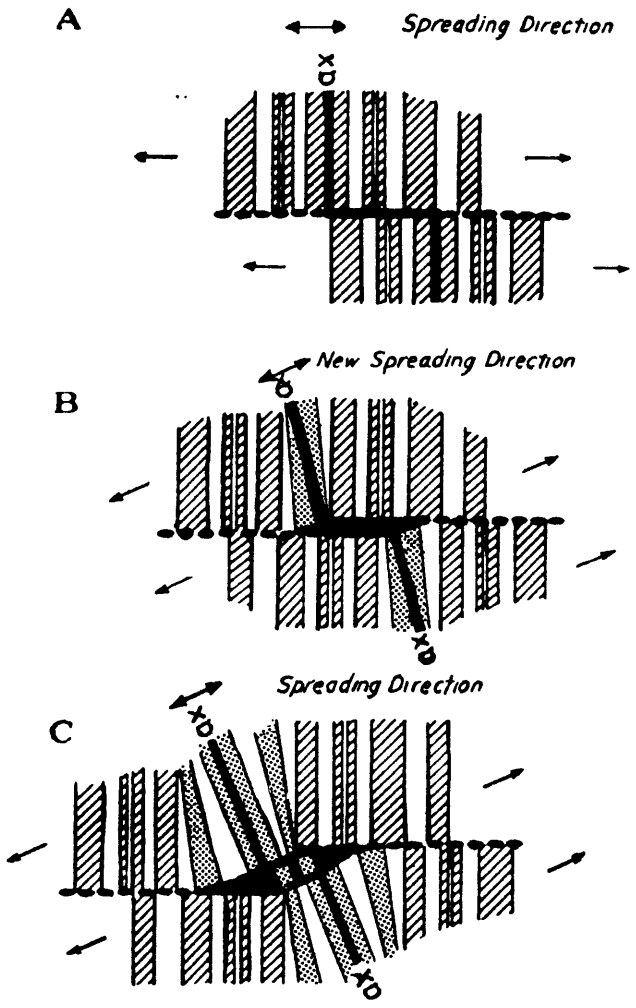
A
Spreading Direction
xD
B
New Spreading Direction
θ
xD
C
Spreading Direction
xD
xD

Figure 11


SAMPLE
1758
1953
2148
2344
2539
2734
2929
0.90
1.00
1.10
1.20
1.30
1.40
1.50
TIME (SECS)

Figure 12

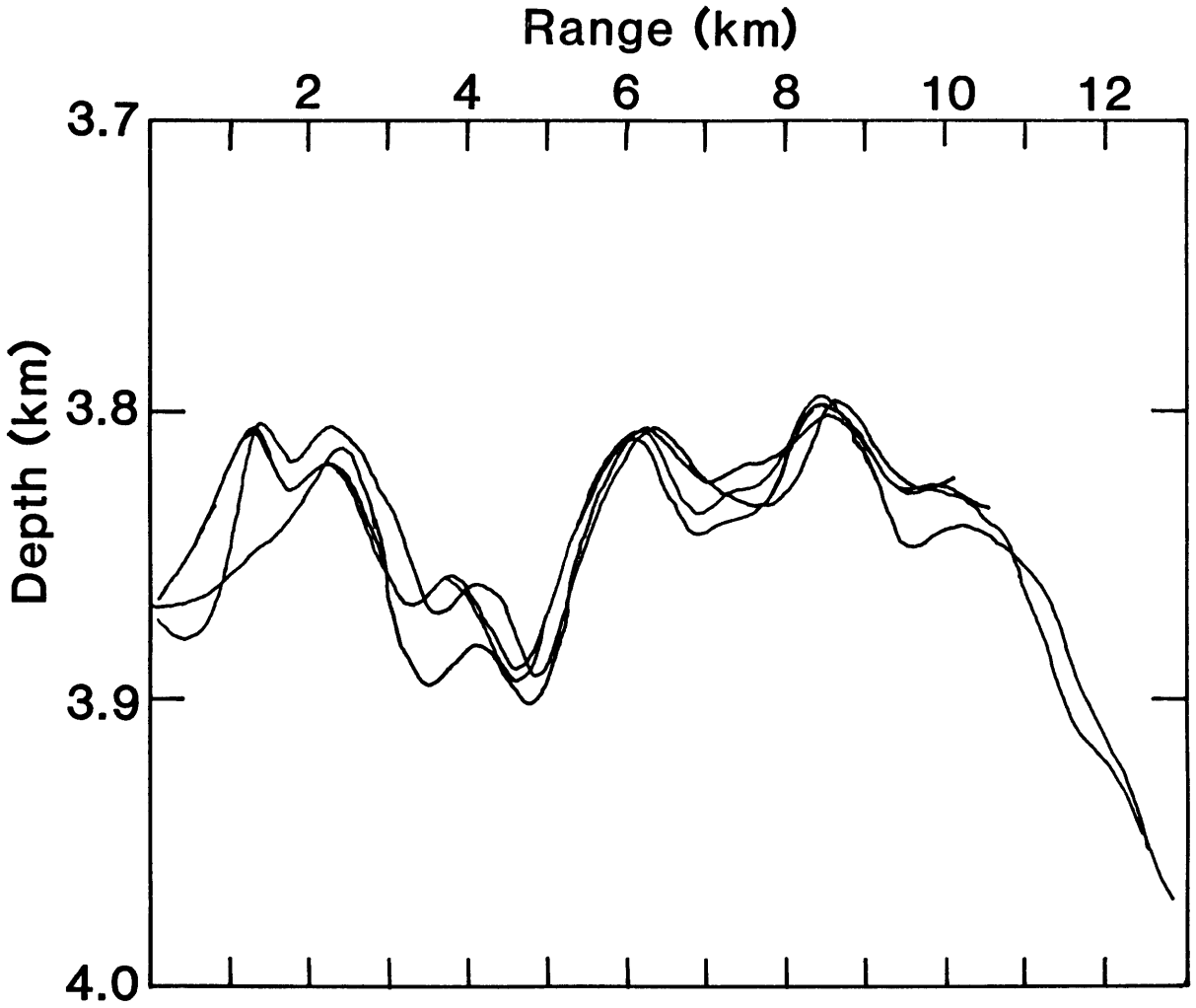

Figure 13

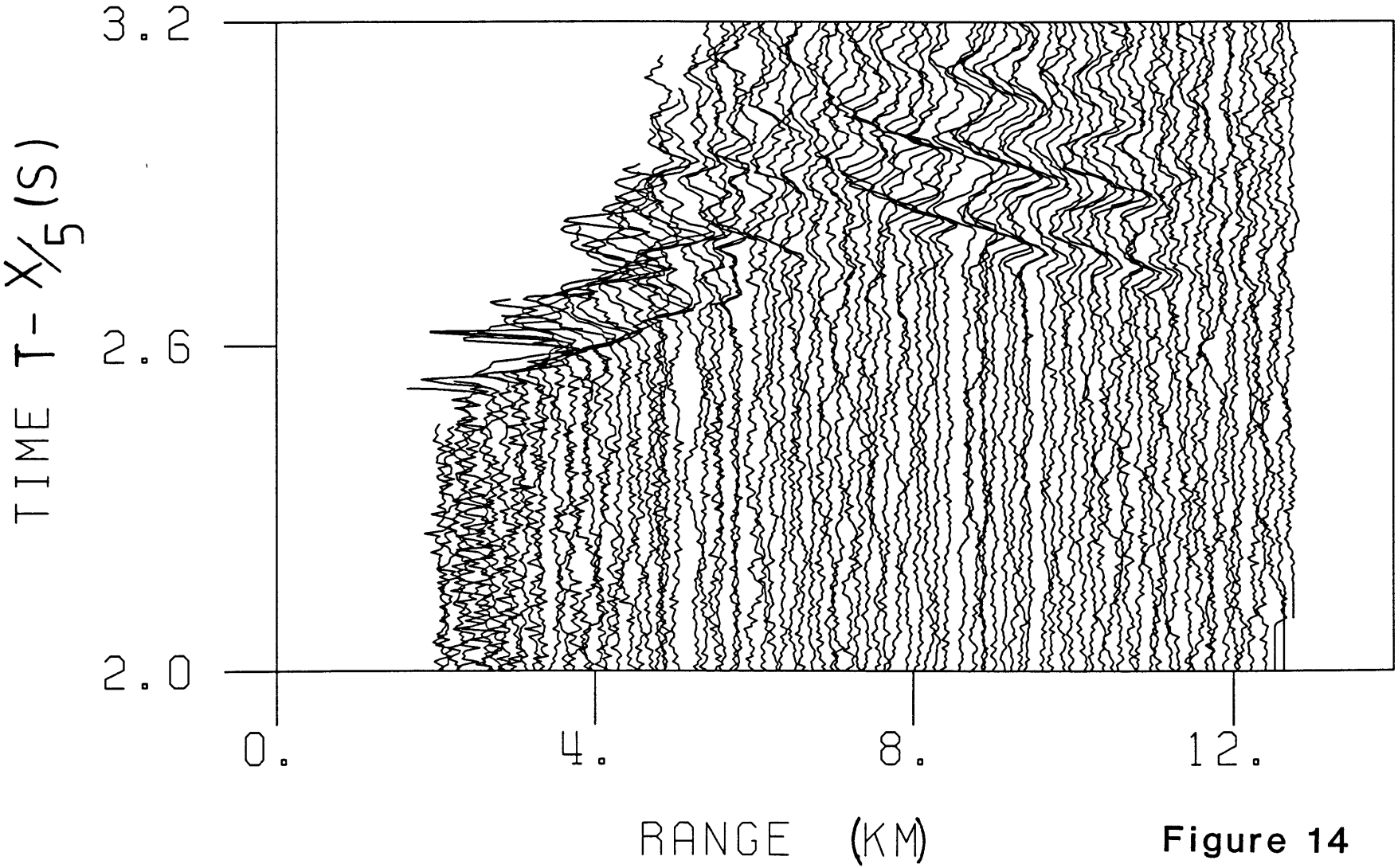

Figure 14

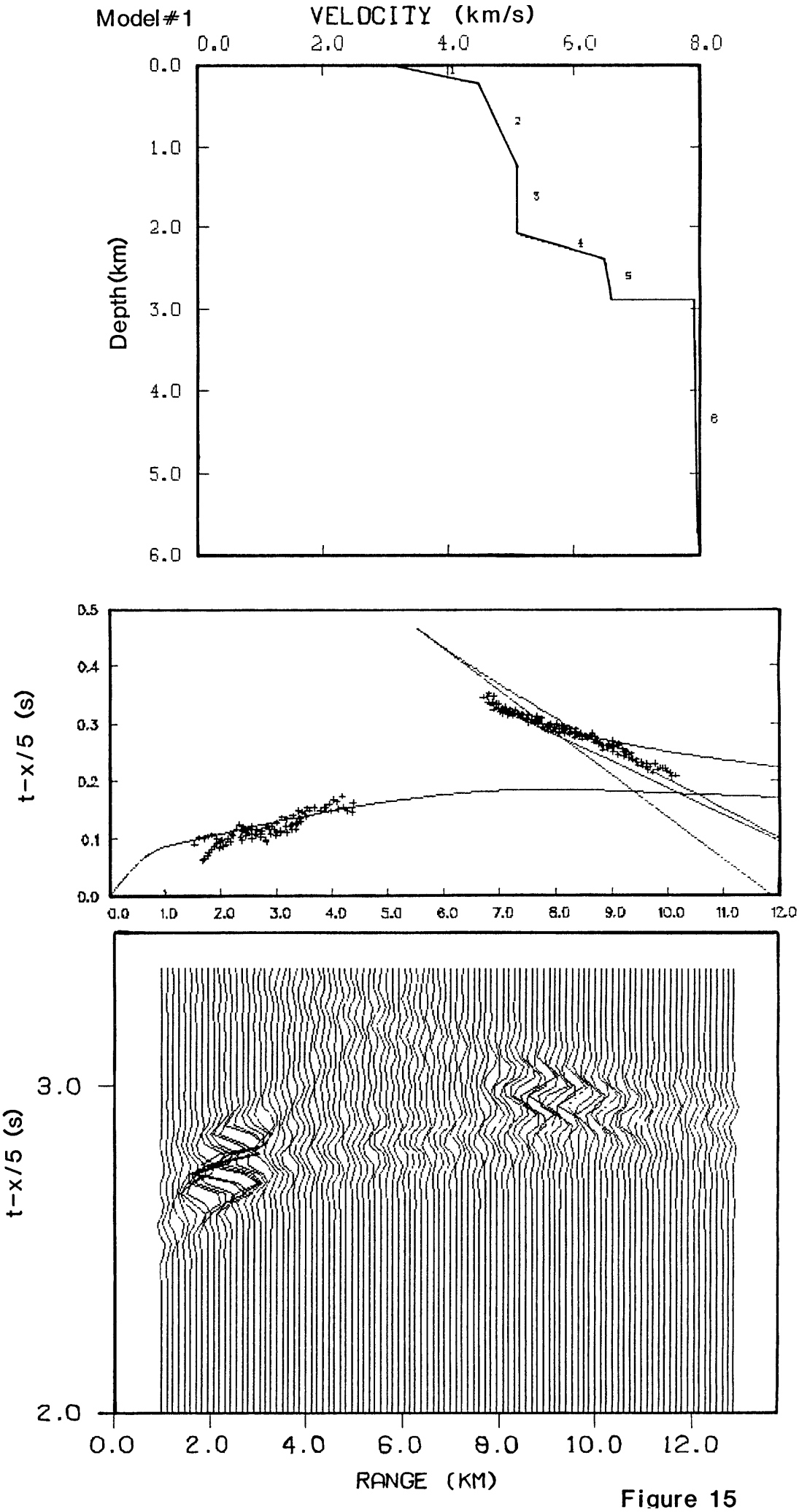
Model#1
VELOCITY (km/s)
0.0
2.0
4.0
6.0
8.0
Depth(km)
1.0
2.0
3.0
4.0
5.0
6.0
1
2
3
4
5
6
t-x/5 (s)
0.5
0.4
0.3
0.2
0.1
0.0
7.0
8.0
9.0
10.0
11.0
12.0
3.0
2.0
RANGE (KM)

Figure 15

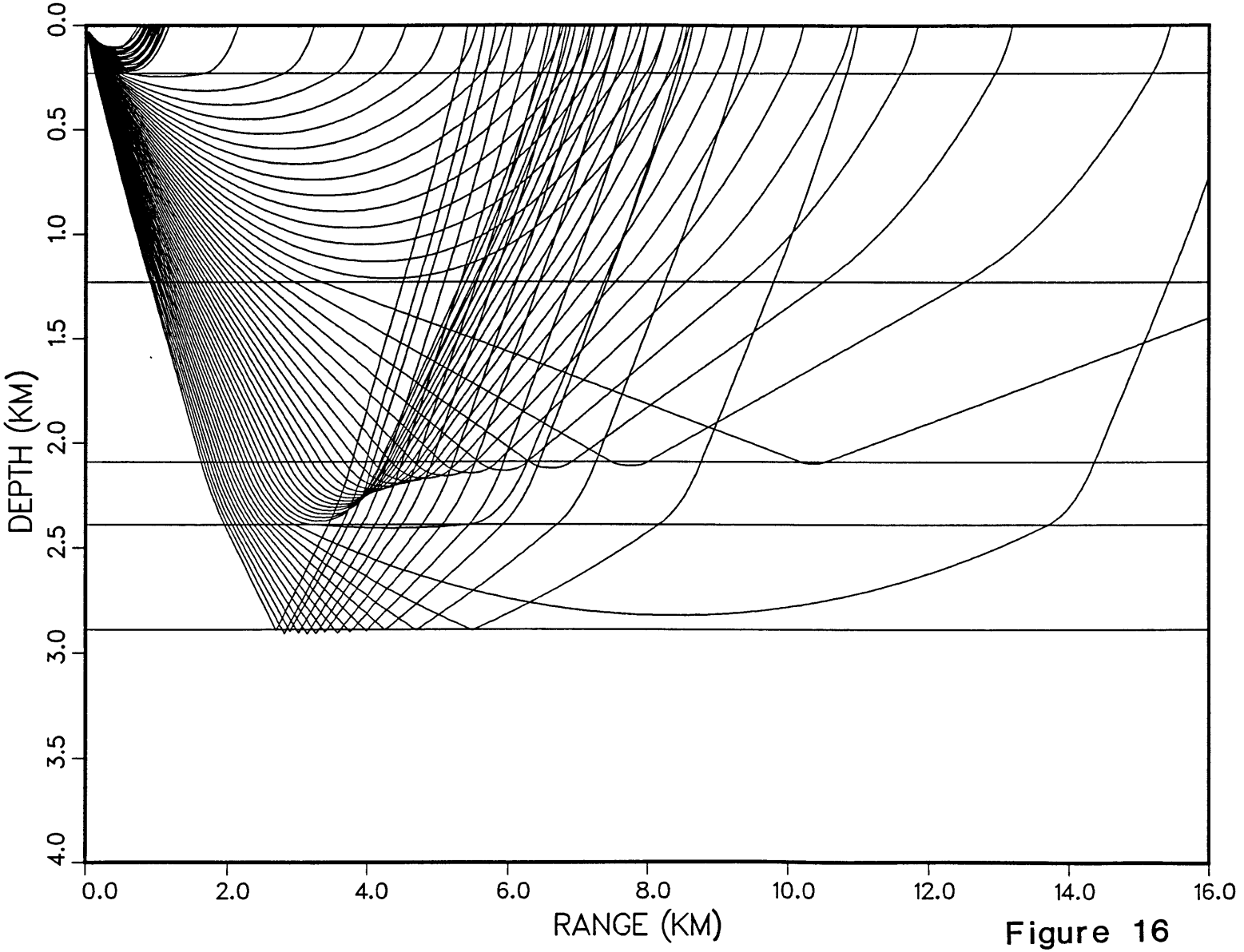
DEPTH (KM)
0.0
0.5
1.0
1.5
2.0
2.5
3.0
3.5
4.0
0.0
2.0
4.0
6.0
8.0
10.0
12.0
14.0
16.0
RANGE (KM)

Figure 16

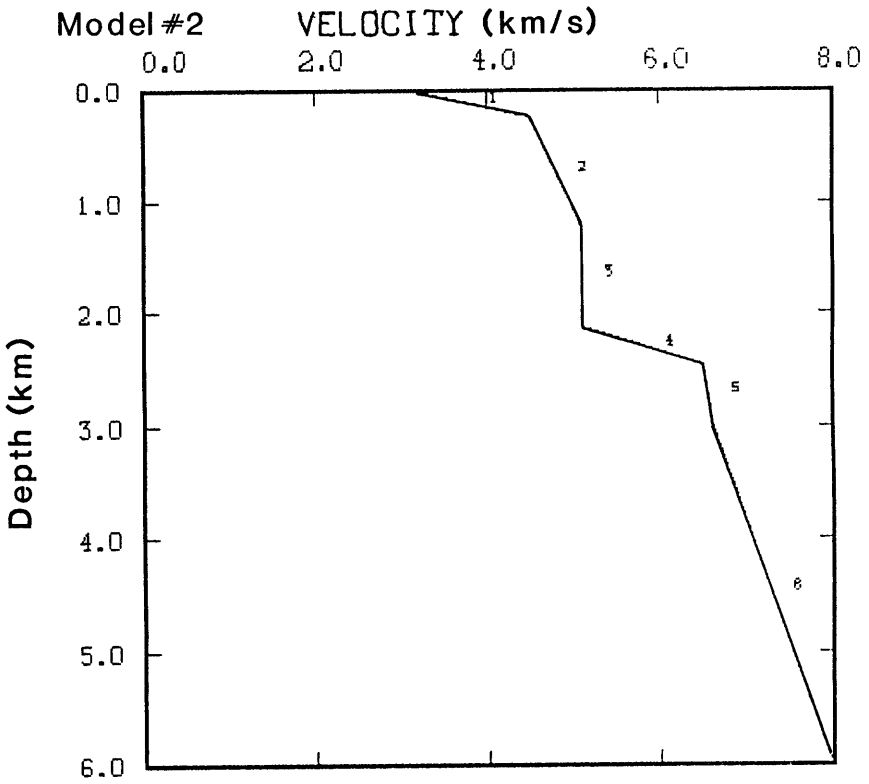
Model #2
VELOCITY (km/s)
0.0
2.0
4.0
6.0
8.0
Depth (km)
0.0
1.0
2.0
3.0
4.0
5.0
6.0
1
2
3
4
5
6

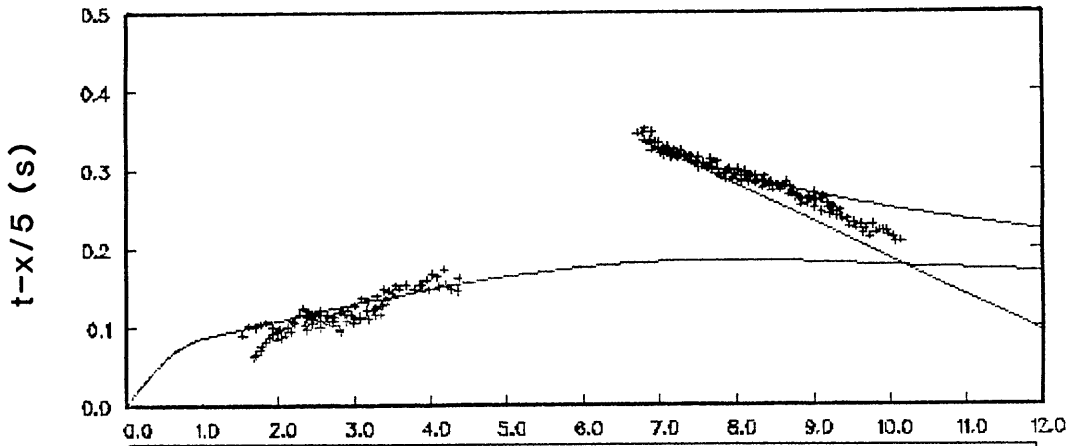
t-x/5 (s)
0.5
0.4
0.3
0.2
0.1
0.0
0.0
1.0
2.0
3.0
4.0
5.0
6.0
7.0
8.0
9.0
10.0
11.0
12.0

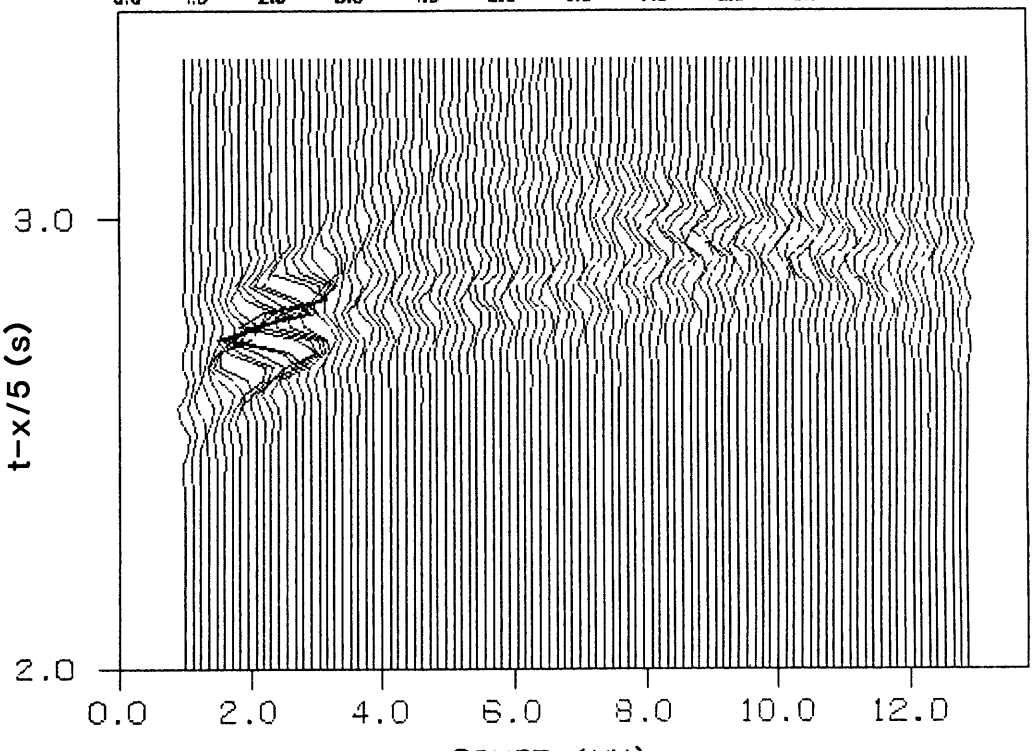
t-x/5 (s)
3.0
2.0
0.0
2.0
4.0
6.0
8.0
10.0
12.0

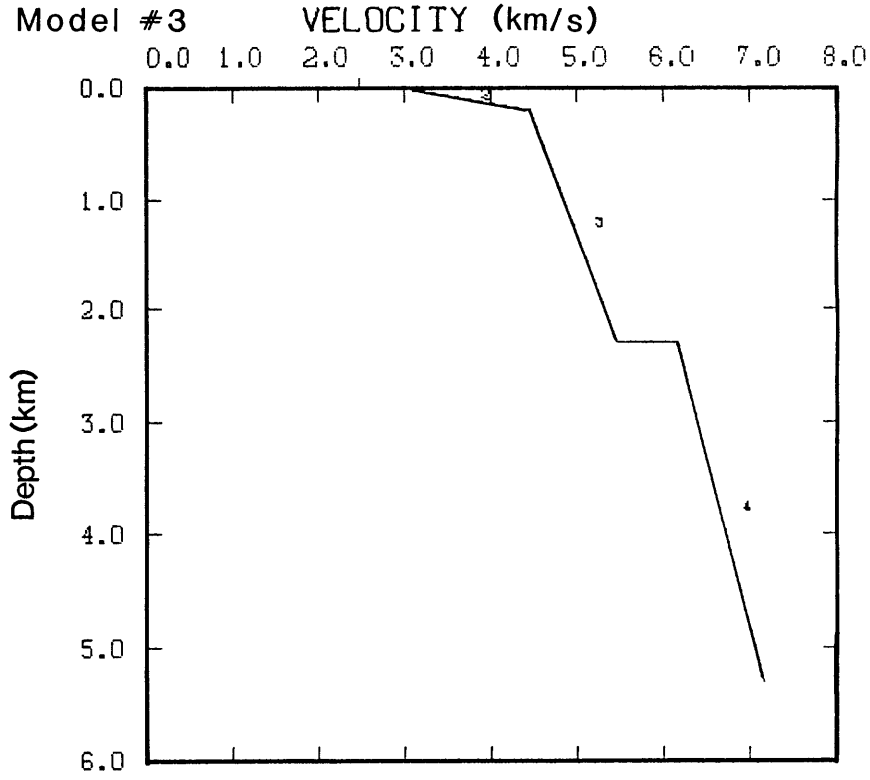
Model #3
VELOCITY (km/s)
0.0 1.0 2.0 3.0 4.0 5.0 6.0 7.0 8.0
Depth (km)
0.0
1.0
2.0
3.0
4.0
5.0
6.0
3
4

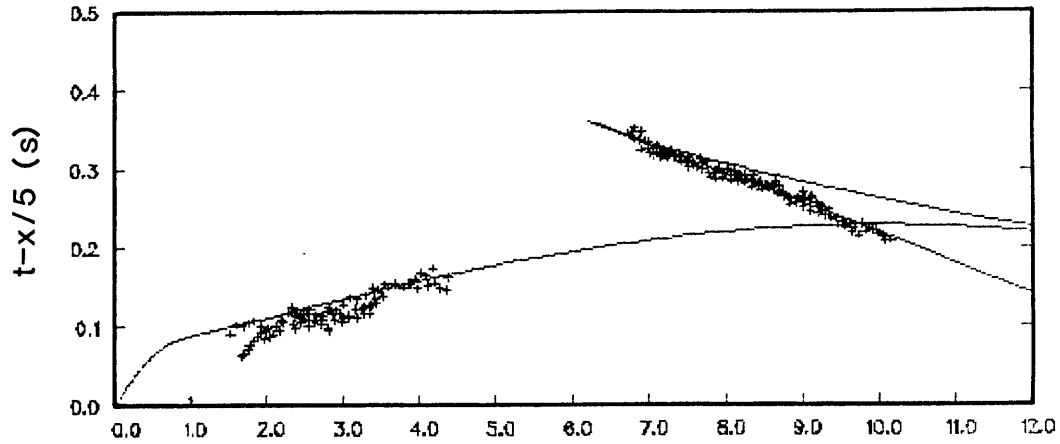
t-x/5 (s)
0.5
0.4
0.3
0.2
0.1
0.0
0.0 1.0 2.0 3.0 4.0 5.0 6.0 7.0 8.0 9.0 10.0 11.0 12.0

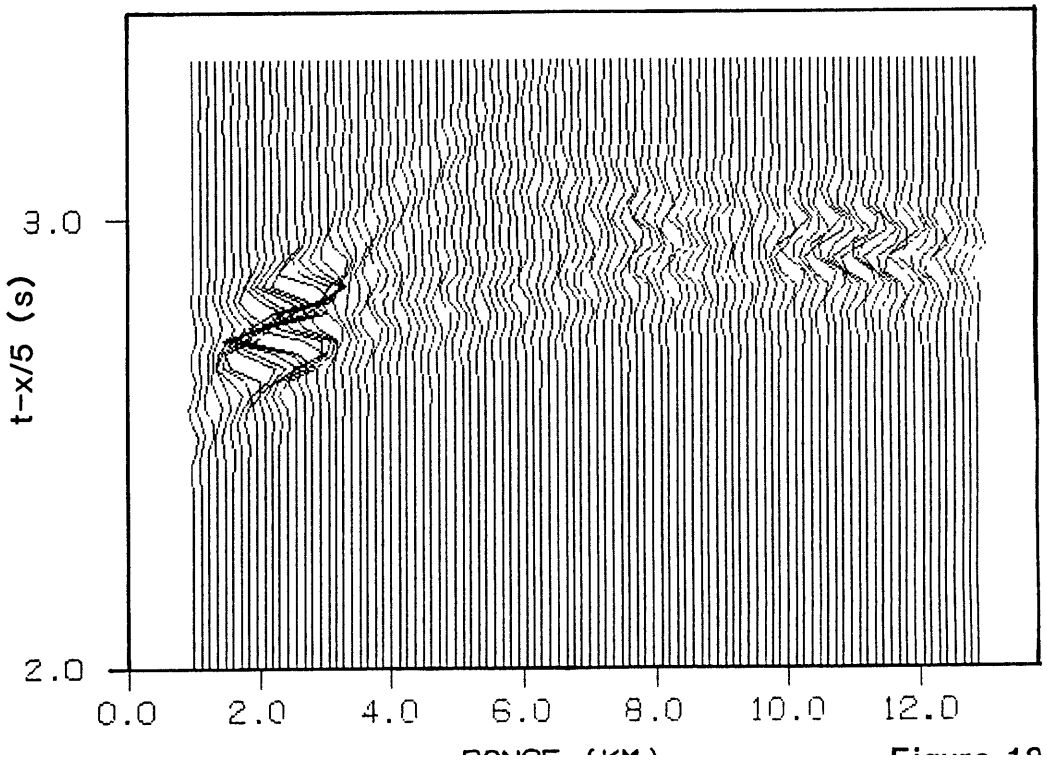
t-x/5 (s)
3.0
2.0
0.0 2.0 4.0 6.0 8.0 10.0 12.0

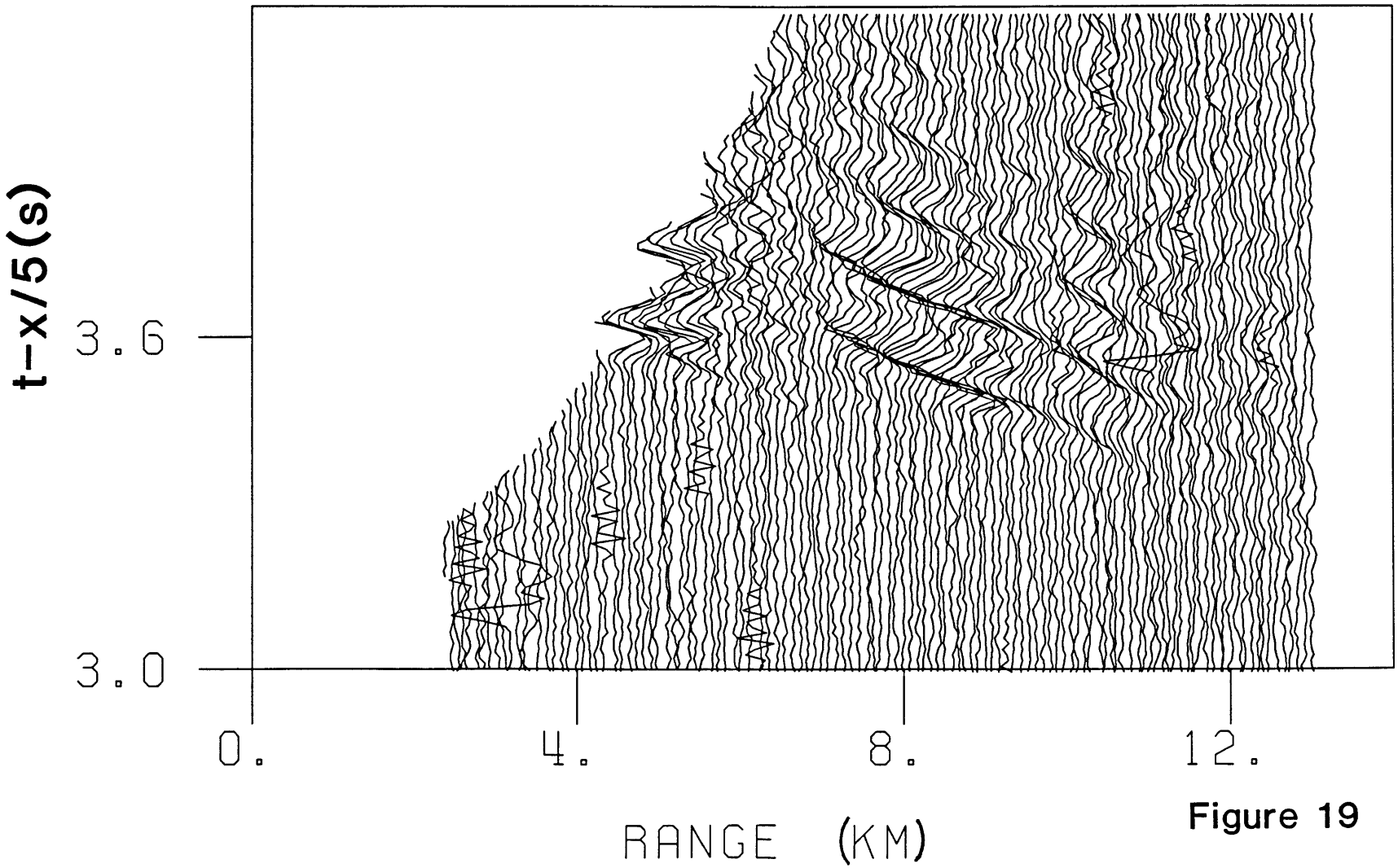

Figure 19

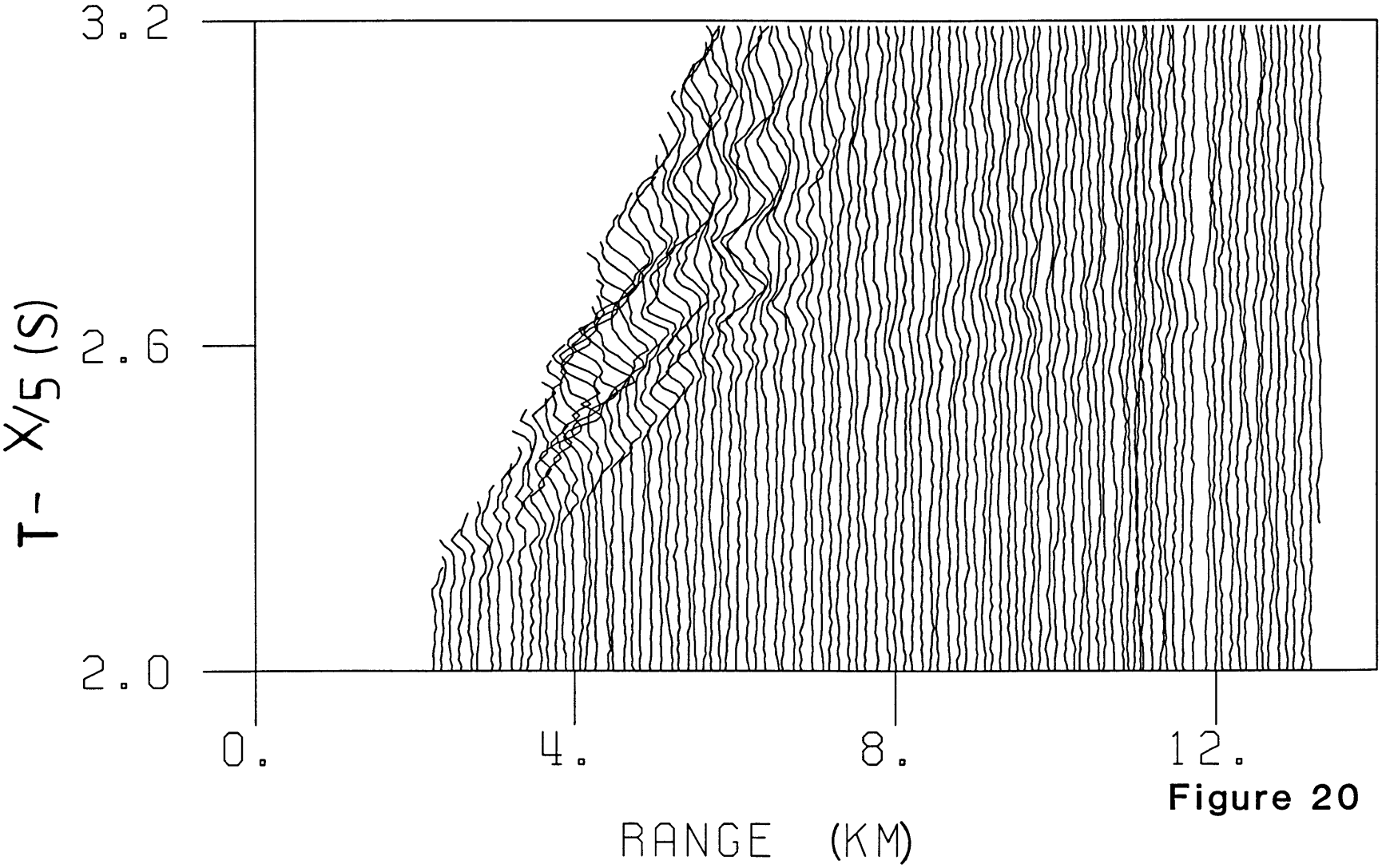

Figure 20

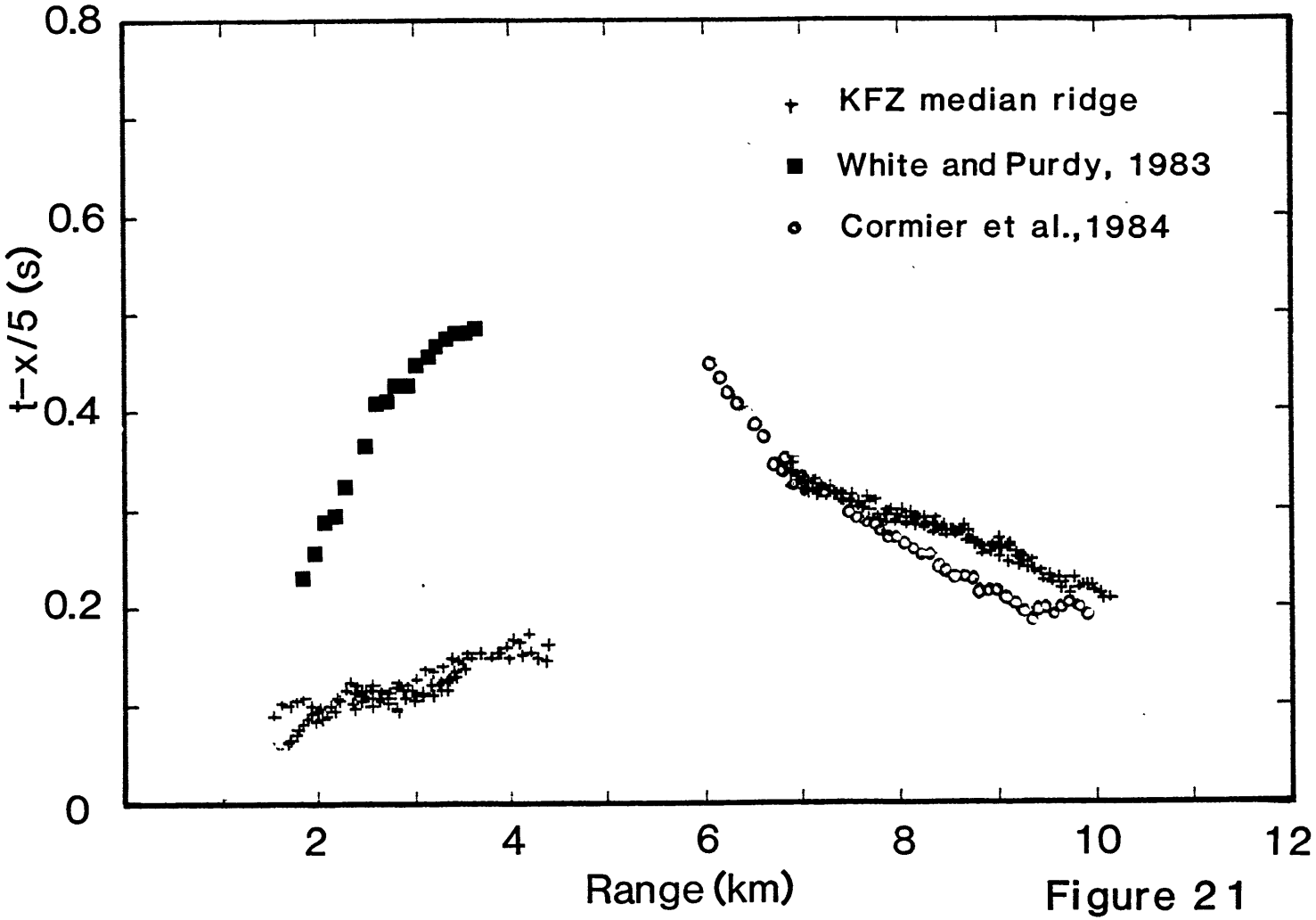
0.8
0.6
0.4
0.2
0
t-x/5 (s)
2
4
6
8
10
12
Range (km)
KFZ median ridge
White and Purdy, 1983
Cormier et al.,1984

Figure 21

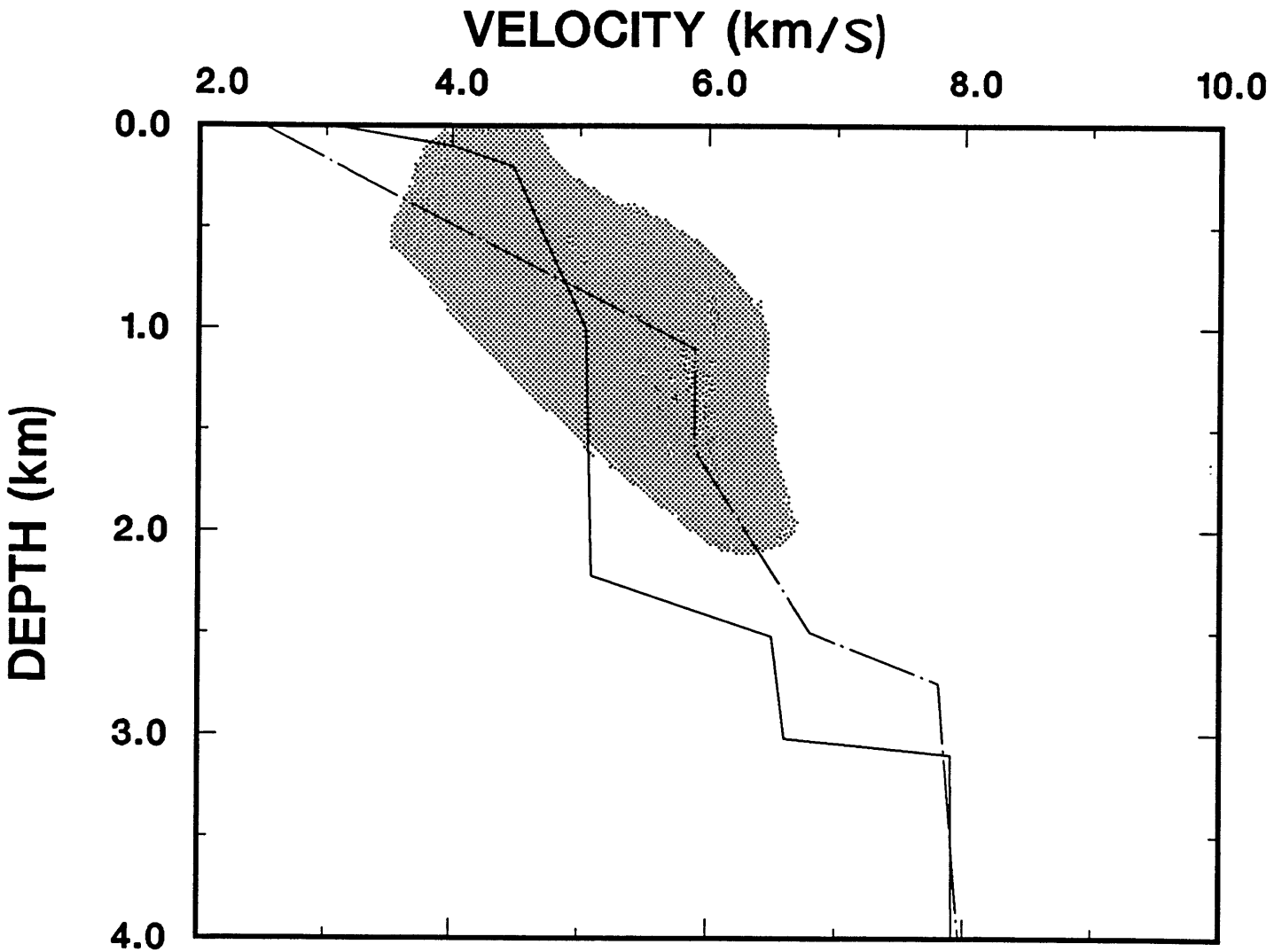

Figure 22